Science of the Total Environment 693 (2019) 133571

Contents lists available at ScienceDirect

Science of the Total Environment

journal homepage: www.elsevier.com/locate/scitotenv

Streamflow calculation for medium-to-small rivers in data scarce inland areas

C.S. Zhao [a,b,e], T.L. Pan [b], J. Xia [c,*], S.T. Yang [a,b], J. Zhao [d], X.J. Gan [d], L.P. Hou [b], S.Y. Ding [d]

[a] College of Water Sciences, Beijing Normal University, Beijing Key Laboratory of Urban Hydrological Cycle and Sponge City Technology, Beijing 100875, PR China
[b] School of Geography, Faculty of Geographical Science, Beijing Normal University, Beijing 100875, PR China
[c] State Key Laboratory of Water Resources & Hydropower Engineering Sciences, Wuhan University, Wuhan 430072, PR China
[d] Jinan Survey Bureau of Hydrology and Water Resources, Jinan 250013, PR China
[e] ICube, UdS, CNRS (UMR 7357), 300 Bld Sebastien Brant, CS 10413, 67412 Illkirch, France

HIGHLIGHTS

- We present a new framework to estimate river discharge in inland data-scarce areas.
- It yields a significantly higher accuracy for river discharge estimation.
- It can promote researches of inland stream flow estimation worldwide.

GRAPHICAL ABSTRACT

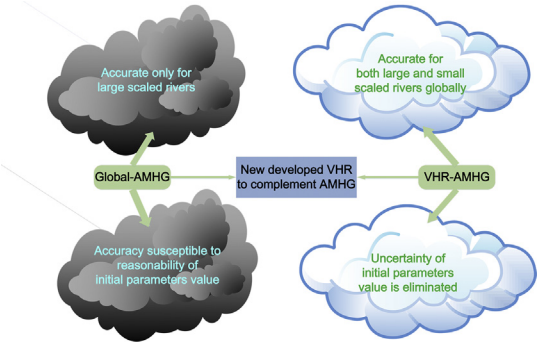

ARTICLE INFO

Article history:
Received 6 May 2019
Received in revised form 24 June 2019
Accepted 22 July 2019
Available online xxxx

Editor: Ralf Ludwig

Keywords:
Inland streamflow estimation
Medium-to-small rivers
Data-scarce area
UAV

ABSTRACT

Inland streamflow estimation is essential in global water supply and environment protection. In data-scarce areas a highly efficient way of estimating streamflow is through remote sensing methods. However, high requirement of most previous methods on ground-measured data hinder their wide use in data-scarce areas. Therefore, this paper presented a new framework for estimation of streamflow in medium-to-small rivers with few ground measurements by using high-resolution unmanned aerial vehicle (UAV) imagery. A new Virtual Hydraulic Radius (VHR) method was proposed to complement AMHG (at-many-stations hydraulic geometry), a method not requiring any ground measurements when global parameters are used (global–AMHG) in large-scaled rivers but yielding great uncertainties in smaller scaled rivers, thus creating a VHR-AMHG method for medium-to-small rivers. The accuracy verification of the proposed method was performed by comparing it to field measurement data and the global parameters of the original AMHG (global–AMHG). Results showed that the root mean square error calculated from VHR-AMHG was 32.15 m^3/s, while that from global–AMHG was 305.65 m^3/s, indicating that the VHR-AHRG method yields a significantly higher accuracy for streamflow estimation for medium-to-small rivers. We found that regardless of the size of the river, AMHG is not applicable for rivers having excessively small b values in the equation $w = aQ^b$ (low-b rivers). For medium-to-small rivers with $b < 0.25$, AMHG is not recommended. The accuracy of the original AMHG method is limited by the initial value of the model parameters and the condition that the congruent discharge (Q_c) has to be within the range of observational discharge. The initial value setting of the model parameters significantly impacts the calculation accuracy. The VHR-AMHG

* Corresponding author at: Wuhan University, Wuhan 430072, PR China.
E-mail address: xiajun666@whu.edu.cn (J. Xia).

https://doi.org/10.1016/j.scitotenv.2019.07.377

method is able to overcome the deficiencies of the original AMHG, i.e. being overly dependent on the initial value setting with long-series known discharge data. It also eliminates the limitation of the Q_c condition, as it achieves a higher accuracy for rivers in which Q_c does not satisfy the condition compared to using global-AMHG on rivers that actually meet the condition, thus greatly expanding its usage scope. Thus VHR-AMHG method can provide detailed data on the spatial and temporal distribution of regional and national streamflow for governments and stakeholders, and offer scientific data support for wisely making water supply polices and sustainably protecting eco-environment.

1. Introduction

Inland rivers are closely connected to human survival, human activities, and regional ecological environments (Escartin and Aubrey, 1995; Ruiz et al., 2004; Zhou and Broodbank, 2014). Streamflow (or river discharge) plays an indispensable role in maintaining the stability of the hydrosphere system and eco-environment. The methods measuring streamflow are increasingly diverse (Durand et al., 2014; Legleiter et al., 2017); however, streamflow estimation remains plagued by problems related to geography, funds, and other factors (Pan et al., 2016). Traditional measurement is time-consuming and unable to provide a solution for data-scarce areas with either no survey stations or insufficient data. In addition, it is difficult to apply such methods to non-contact discharge measurements, such as for environmental disaster response and emergency monitoring (Le Coz et al., 2010; Lee et al., 2002). Therefore, a rapid and accurate method for streamflow estimation is urgently needed for data-scarce areas.

Inversion methods of streamflow estimation, with remote-sensing technology being the most representative method, are products of in-depth research in the fields of computer science and spatial science during recent years. Using these methods, researchers are able to perform the inversion of discharge under difficult geology and harsh conditions without gauging the water (Hirpa et al., 2013). There are two main types of inversion methods: near-surface remote sensing and satellite remote sensing. Near-surface remote sensing mainly includes stereo vision—particularly imaging (Li, 2016), Doppler radar and ground penetrating radar (Costa et al., 2006; Costa et al., 2000), aircraft–radar–water surface elevation (LeFavour and Alsdorf, 2005), water-level/slope/hydraulic method (Jung et al., 2010; Bjerklie et al., 2018), etc. However, the expensive instruments limit the wide application of such methods. In contrast, satellite remote-sensing methods have the advantages of low cost, high speed and convenience, and ease of implementation. They have been widely used in large rivers and can be approximately divided into five types: water surface area (satellite–water surface area), water surface width (satellite–water surface width), water level (satellite–water level) and hydrological multi-parameter set (satellite–multiparameter), and coupling of satellite data and hydrological model (satellite–hydrological model).

The satellite–water surface area method uses ERS-1 radar satellite images and simultaneous ground measurement data to establish a correlation between water surface area and discharge for the inversion of streamflow (Smith et al., 1996; Smith et al., 1995; Song et al., 2011). The satellite–water surface width method uses water surface width information obtained from satellite images such as QuickBird-2 together with fitting curves generated from survey stations to invert streamflow (Pavelsky et al., 2014; Xu et al., 2004). The satellite–water level method converts the information on the underlying surface water level estimated using TOPEX/Poseidon satellite data into a series of water level values. It establishes the relationship between the water level values from satellite data and the measured discharge from adjacent hydrological stations. Thus, the discharge can be estimated using TOPEX/Poseidon (TP) satellite data (Zhang et al., 2002; Zhang et al., 2004) or by directly using satellite altimetry data of TP, ERS-2 and ENVISAT, etc., to estimate discharge for areas with no data (Getirana and Peters-Lidard, 2013; Papa et al., 2010). The satellite–multiparametric method measures hydrodynamic and hydrological parameters such as water surface width, hydraulic gradient, and water level to invert the discharge of large rivers with widths > 100 m (Biancamaria et al., 2016; Birkinshaw et al., 2014; Durand et al., 2016; Gosling and Arnell, 2011; Pavelsky et al., 2014). Alternatively, it calculates water cycle components from satellite inversions by linking remote sensing and synchronized ground measurement (Li et al., 2012; Lu et al., 2010). The satellite–hydrological modeling method combines satellite data, surface climate data, and hydrological modeling to measure the discharge of large rivers (Andreadis et al., 2007; Vörösmarty et al., 1996).

Among the five methods previously described, most are highly dependent on ground measurement data, whereas the global parameters in at-many-stations hydraulic geometry (AMHG) is one of McFLI (Gleason et al., 2016). It calculates the streamflow solely from the variation in river width, making it among the mainstream methods widely used for streamflow estimation via remote sensing (Bonnema et al., 2016; Durand et al., 2016; Gleason et al., 2014; Gleason et al., 2018). However, satellite-induced scale problems (Wu and Li, 2009), restricted its wide application in medium and small rivers. In other words, because of the limitations of satellite spatial resolution, the accuracy of this method is relatively high for large rivers (average river width ≥ 500 m) but unstable for medium-to-small rivers (average river width ≤ 250 m) (Gleason et al., 2014), thus greatly limiting its application to medium-to-small rivers lacking hydrological monitoring data. Therefore, there is an urgent need to explore new methods to enhance the AMHG method and to expand the scope of its application.

The effective management of medium-to-small rivers is of great significance for improving flood control capacity, optimizing water ecological environments, driving economic and social development along rivers, and promoting the harmonious coexistence between human and nature (Pawłowski et al., 2016; Pawłowski et al., 2015). However, medium-to-small rivers usually lack surface hydrological monitoring stations, and without sufficient data, it is difficult for satellites to accurately measure the width of medium-to-small rivers. Furthermore, the data acquisition of high-resolution satellites is limited by factors such as funds, time, government policies, and geography, which pose difficulties for the popularization and application in practical situations and thus considerably limit the application of the satellite-based AMHG method. Compared to satellite remote sensing, low-altitude unmanned aerial vehicle (UAV) remote sensing boasts the advantages of high flexibility, convenience, and high speed and resolution. The pixel size can be controlled by the flight altitude, therefore this method is suitable for river sections at various scales (large, medium, and small). As such, it has become among the major low-altitude remote-sensing platforms available today (Colomina and Molina, 2014; Watts et al., 2012). It is widely used in the monitoring of river morphology, soil erosion, dynamic topography (Cho et al., 2015; Lee and Choi, 2015; Neugirg et al., 2016), ecological parameter acquisition (Vivoni et al., 2014), and disaster response (Li et al., 2008). UAVs acquire river data at a centimeter resolution, and data acquisition can be performed at any time. Upon combination with the AMHG method, the accuracy of the discharge estimation of medium-to-small rivers can be substantially improved.

The objective of this paper is to present a new framework for estimation of streamflow (or river discharge) in data-scarce areas. We proposed a novel method to calculate medium-to-small streamflow based on high-resolution UAV remote-sensing images so as to provide prior knowledge for AMHG when applied to data-scarce medium-to-small rivers. The accuracy of the novel method was further verified by comparison of field-measured data with the global parameters of the original method. Possible methods for eliminating the application limitations of the original AMHG method were also explored.

2. Study area

With an area of 8177.21 km^2, Jinan (latitude 36.0°–37.5°, east longitude 116.2°–117.7°) is the first pilot city for China project to build cities with healthy water ecological communities. It is south of Taishan Mountain and within the three major fluvial systems of the Yellow, Haihe, and Huai Rivers. The Yellow, Tuhai-Majia, and Xiaoqinghe rivers run through the city. The climate is cold and dry during winter and hot and humid during summer. The average annual precipitation is 619.7 mm; however, the annual precipitation significantly varies year-by-year and is unevenly distributed during the year. Rainfall is mainly concentrated during the flood season from July to September, with precipitation during this period accounting for 50% to 70% of the annual precipitation (Bi et al., 2007). The main source of river runoff is rainfall, with the scarcity of rainfall during the non-flood season and the continuous usage of water resources often leading to zero discharge, while intense flooding during the flood season results in a sharp increase in discharge. Both situations pose an unprecedented threat to the sustainable development of the local society and economy. Currently, there are only three hydrological stations in the entire study area. As such, hydrological monitoring of the medium-to-small rivers is insufficient, making it difficult to implement effective measures to prevent floods in advance and to manage and/or control losses. In the present study, based on the control sections of nine typical medium-to-small rivers in Jinan, UAV flights and ground measurements sampling were performed, and historical discharge data of the hydrological stations were collected. Ground-measured discharge and cross-section data were used to verify the reliability of the AMHG and analyze the accuracy of the new method.

3. Data and methods

3.1. Data

3.1.1. UAV imaging data

To study the accuracy of AMHG when applied to medium-to-small rivers and explore improvement methods, ten large-scale field surveys of the entire study area was carried out from 2014 to 2016. The UAV flew across nine rivers (for one particular river, a total of 11 river segments in the upper, middle, and lower reaches were covered) and collected a total of 2477 photographs. From 200 to 300 images per station were taken using a controlled flight method, with the photograph shooting overlap rate set to 90% so as to ensure the accuracy of the subsequent software-generated data such as stereo image pair, point cloud, and digital surface model (DSM) datasets, which are generated in Pix4dMapper Software (Version 2.0.104). The generated DSM had a spatial resolution of from 2.22 cm (flight altitude: 50 m) to 4.23 cm (flight altitude: 100 m) (Zhang et al., 2018).

The basic parameters of the UAV are shown in Table 1. The flight control software used was Pix4Dcapture developed by Pix4D S.A. (https://pix4d.com/).

3.1.2. Ground data

During the flight of the UAV, discharge data was simultaneously measured on the ground at each station. In addition, historical data (discharge, cross-section) from the hydrological stations were collected. A total of 27 measurements on ground-measured discharge data and 1 measurement on cross-section data were acquired, specifically, 15 measurements in wet season, 12 measurements in dry season, as shown in Table 2.

Table 1
DJI Phantom-3-pro's basic parameters (Zhang et al., 2018).

Basic parameters of UAV	
UAV product	Phantom-3-pro
Camera	FC300X
Camera sensor	Sony Exmor R CMOS
Max photo resolution	4000 × 3000
Max aperture	f/2.8
Focal length	20 mm
Field of view (FOV)	94°
Max flight altitude	500 m
Max flight time	23 min

3.2. Methods

AMHG method was firstly introduced before a new method – Virtual Hydraulic Radius (VHR) method to produce prior knowledge whereby to estimate initial values for AMHG was introduced. Secondly, a method to estimate AMHG parameters with initial values was presented. Finally, methods for sensitivity test and error assessment were introduced.

To facilitate quantitatively evaluating accuracy of the AMHG for medium-to-small streamflow calculation, two scenarios were set as follows: (1) calculation of streamflow based on parameter provided by VHR method, and (2) calculations based solely on the global parameters provided by Gleason and Wang (2015) without the use of hydrological data. The technology roadmap for this study is shown in Fig. 2.

3.2.1. AMHG

The AMHG, the core method of this paper, is derived from the traditional AHG (at-a-station hydraulic geometry). For AHG, there are three empirical relationships: width–AMHG (Eq. (1)), depth–AMHG (Eq. (2)), and velocity–AMHG (Eq. (3)) as follows:

$$w = aQ^b \tag{1}$$

$$d = cQ^f \tag{2}$$

$$v = kQ^m \tag{3}$$

where w is the river width (m); d is the river depth (m); v is the river flow rate (m/s); Q is the streamflow (m^3/s); and a, b, c, f, k, m are the empirical parameters (Leopold and Maddock, 1953). AMHG demonstrates that within the three empirical relationships, the parameters a and b, c and f, and k and m are not completely independent; instead, they are linked by log-linear correlations along the river (Gleason et al., 2014).

Table 2
Ground-measured data.

Basin	Stations	Data
Yellow River Basin	LK	Discharge (1 measurement, wet season)
	CT	Discharge (1 measurement, wet season)
	ZK	Discharge (1 measurement, wet season)
	BDK	Discharge (1 measurement, wet season)
	BDSH	Discharge (1 measurement, wet season)
Hai River Basin	ZGNL	Discharge (1 measurement, wet season)
	LJB	Discharge (1 measurement, wet season)
	LCQ	Discharge (1 measurement, wet season)
Huai River Basin	WLT	Discharge (19 measurements, 12 measurements in dry season, 7 measurements in wet season)
		River width (19 measurements)
		Cross-section (1 measurement)

Although in principle any of a river's three AMHG relationships may be used, we herewith focused on the width–AMHG relationship, similar to that in Gleason and Smith (2014), as unlike river depth or velocity, river width is straightforward to measure via multiple UAV imaging.

Gleason and Wang (2015) give a derivation of AMHG and show that it arises because individual AHG curves intersect at the same point in hydraulic space (e.g. the same values of width and discharge). It is the width-AMHG that enables remote sensing of discharge, which is formulated as:

$$b = -\frac{1}{\log(Q_c)} * \log(a) + \frac{1}{\log(Q_c)} * \log(w_c) \quad (4)$$

where $1/\log Q_c$ and $\log w_c/\log Q_c$ respectively represent two important parameters, AMHG slope, AMHG intercept as described by Gleason and Smith (2014). Note that Eq. (4) are special cases of Eq. (1) when AMHG is observed, yet they hold simultaneously at all stations of a river, not just a single station as in Eq. (1). Gleason and Wang (2015) then posited that w_c can be given by the spatial modes of time mean quantities of width, which is further proved by Shen et al. (2016). However, the physical hydraulic quantity to which Q_c corresponds has yet to be uncovered, Gleason et al. (2018) took long-term mean of P-ET satellite water balance as priori estimate to characterize Q_c. In this study, instead of using satellite-model estimation of discharge, we use VHR method mentioned in Section 3.2.2 to generate priori estimation of discharge based on UAV imagery, then taken the time mean of discharge as Q_c.

Gleason and Smith (2014) were able to simplify Eq. (1) by replacing b with a function of log(a), as provided by Eq. (4). This simplification reduces the number of unknown parameters in Eq. (1) from 2n + 1 to n + 1 for any n cross sections in a mass conserved reach, as Q is equivalent in such cross sections and W is easily given by remotely sensed observations. This simplified system of AHG curves per cross section is then sufficient for unconstrained, and genetic algorithm was introduced to heuristically optimize unknown parameters in Eq. (1) for solving Q (Gleason and Hamdan, 2015).

Parameter calibration plays a critical role in the accuracy of the results of hydrological calculations (Chlumecký et al., 2017). Commonly used automatic optimization algorithms for model parameters include the genetic algorithm (GA), simplex algorithm (SM) (Tsoukalas et al., 2016), and the Rosenbrock Algorithm (Nicolle et al., 2014), with GA being more recognized than others (Chlumecký et al., 2017). Previous experiments have shown that it yields better results in parameter calibration (Horton et al., 2017).

Simply stated, GAs are probabilistic search procedures designed to work on large spaces involving states that can be represented by strings (Goldberg and Holland, 1988; Iqbal et al., 2018). To solve the target optimization problem and to ensure global convergence, GAs also incorporate elitist selection strategies (De Jong, 1975; Li et al., 2016) using objective functions to evaluate fitness and retain individuals with better fitness. This has a major impact in improving the global convergence of standard GAs and compensates for the deficiency in convergence to local optimal solutions (Feng et al., 2017; Rudolph, 1994).

In the present study, the root mean square error (RMSE) was set as the objective function for GAs. Based on the principle of a minimum RMSE, individuals were selected for crossover and mutation. The RMSE calculation method is shown in Eq. (5) as follows:

$$RMSE = \sqrt{\frac{\sum_{i=1}^{n}(X_i - Y_i)^2}{n}} \quad (5)$$

In this study, X_i is the simulation value of discharge; Y_i is the ground-measured. A GA was used to obtain the optimized parameters for the AMHG. Each GA seeks to minimize the difference in discharge between cross sections in a pairwise permutation (Gleason et al., 2014). Parameters under the scenario with the lowest RMSE were then used by the AMHG to estimate the reach-averaged discharge.

3.2.2. Virtual hydraulic radius (VHR) method

In order to produce initial parameter values for AMHG, this section developed a new VHR method. When historical discharge and cross-section data are lacking, the adoption of global parameters proposed by Gleason and Wang (2015) to calculate streamflow is the only viable alternative. However, the use of global parameters does not always yield accurate results (Gleason et al., 2014). Therefore, the present study proposes a novel alternative method, the VHR method, for the calculation of accurate initial values of parameters for the AMHG, which can produce priori knowledge for rivers that lack of historical data.

Regarding the lack of data for medium-to-small rivers, the present study used a UAV to determine the topography above the water surface during the low-flow period. Based on the principle of Manning Equation, the value of R was calculated under the assumption that the actual water surface width was the river bottom forming an incomplete virtual cross-section, and the virtual discharge (Q) was calculated according to the Manning Equation. Q refers to the virtual discharge calculated from the incomplete virtual cross-section, not the actual discharge. As long as a reference station with a complete cross-section was selected in the study area, the equation for determining the real discharge (Q′) from Q could be established to provide the initial value for the six parameters of the AMHG. The minimum and maximum values of Q′ were set as *lowerboundary_Q* and *upperboundary_Q*, respectively. Subsequently, Q′ and the river width measured using the UAV DSM were substituted into Eq. (1) to obtain a and b. The median method was then used to construct the intervals, in which the minimum and maximum values of interval were set as *lowerboundary_a* and *upperboundary_a*, while the minimum and maximum values of interval b were set as *lowerboundary_b* and *upperboundary_b*. The process of deducing the real discharge (Q′) from Q is described as follows:

First, the Manning Equation is introduced as Eq. (6).

$$Q = A \cdot v = \frac{1}{n} A \cdot R^{\frac{2}{3}} \cdot S^{\frac{1}{2}} = \frac{1}{n} A \cdot \left(\frac{A}{P}\right)^{\frac{2}{3}} \cdot S^{\frac{1}{2}} \quad (6)$$

$$Q' = m * Q + n \quad (7)$$

where A is the area of the cross-section (m^2); V is the cross-sectional flow rate (m/s); R is the hydraulic radius (m), which is the ratio of the cross-sectional area A to the wetted perimeter P(m); S is the gradient; and n is the roughness.

In VHR, the wetted perimeter P and the water area A were calculated based on the assumed river bottom, then the hydraulic radius R at different water levels was calculated using the equation R = A/P. The process is shown in Fig. 3a, where the thin red line indicates the assumed wetted perimeter (*VirtualP*) and the thick blue line indicates the true wetted perimeter (*RealP*). Combined with the Manning Equation (Eq. (6)), the virtual discharge (Q) and real discharge (Q′) at different water levels were calculated. Regression analysis was then performed to determine the correlation between Q and Q′ (Eq. (7), Fig. 3b) to deduce the real discharge Q′.where m and n are linear regression coefficients. Using the discharge Q calculated using the VHR method and Eq. (7), the Manning-Equation-based discharge with complete cross-section data or the real discharge Q′ could be obtained. Because of the scarcity of hydrological monitoring stations along medium-to-small rivers, there is usually a lack of cross-section and discharge data for such rivers. To apply this method to the calculation of discharge at actual cross-sections of all rivers using the Manning Equation, a reference station must be selected to determine the initial values of m and n in Eq. (7). Considering that river width is an important characteristic reflecting the discharge size, and that medium-to-small rivers within the same study area have similar cross-section formation mechanisms,

a river width ratio was introduced to obtain the coefficients m and n of other stations, as shown in Eq. (8):

$$\mathrm{WRatio} = \frac{W_1}{W_i}(\mathrm{i} = 1, \ldots, \mathrm{k}) \tag{8}$$

where WRatio is the river width ratio; W_1 is the average river width (m) at the reference station; W_i is the average river width at the other stations, where i represents the station number; and k represents the total number of stations (k is equal to number of rivers we study). By combining Eqs. (7) and (8), a universal equation for estimating the actual discharge at each station was obtained (Eq. (9)) as follows:

$$Q' = WRatio * (m * Q + n) \tag{9}$$

By substituting Q calculated with the VHR method using UAV data into Eq. (9), the real discharge Q′ at all stations in the study area was estimated.

In VHR-AMHG method, the discharge is basically calculated by using river width that is extracted from multiple images, in the case of the inconvenience to conduct multiple field survey, we put up an alternative method to generate multiple synthetic river width by once flight. Based on assumption that streamflow keeps unchanged over short reaches (~10 km) with no tributaries or outflows, with negligible evaporative losses, and with negligible hyporheic exchange (Gleason and Smith, 2014). Gleason and Smith's (2014) assumption suggests that when the water level rise in an upstream cross-section, the magnitude of discharge variation caused by the water level rise in each downstream cross-section should be equal. In this way, after we simulated the water level rise in an upstream cross-section with a step of 0.01 m, discharge variation (ΔQ) in different downstream cross-section can be calculated with Eq. (10).

$$\Delta Q = Q'_{it} - Q'_{0t} = W_{Ratio} * m * Q_{it} = \frac{W_{Ratio} * m * \overline{S^{\frac{1}{2}}} * (\Delta h * i)^{\frac{5}{3}} * \left(W_{surfact,t} + W'_{it}\right)^{5/3}}{n * \left(W_{surface,t} + W'_{it} + 2 * \Delta h * i\right)^{2/3} * 2^{5/3}}$$

$$(\mathrm{t} = 1 \ldots \mathrm{crosssectionNum}) \tag{10}$$

where t represents serial number of the cross-section along the reach; i is the step number of water level rise, $W_{surface,t}$ is the width of cross-section; W_{it}' is the width of the river corresponding to water level rising $0.01 * i$, which can be cubic spline interpolated by topography above the water surface. Based on the principle that ΔQ is equal along the reach, the water level variation in all downstream cross-sections can be simulated with water-level variation in the upstream reference cross-section, thus, this method can produce multiple synthetic width and discharge by once UAV flight.

3.2.3. AMHG parameter estimation with initial values

Because the initial value setting of model parameters has a great impact on the accuracy of the AMHG calculation (Gleason et al., 2014), two scenarios were investigated in the present study: (1) using AMHG parameters generated from priori knowledge and (2) using the global parameters provided by Gleason and Wang (2015), to set the initial AMHG parameter value ranges (threshold values) of AMHG slope, AMHG intercept, Q, a, and b. The priori knowledge, in this paper, by way of Manning Equation and Virtual Hydraulic Radius, were used as the initial estimate for AMHG parameters.

When applying priori knowledge to AMHG, we use [*lowerboundary_slope*, *upperboundary_slope*] as the threshold value of AMHG slope, which is determined by $-1/\log(Q_c)$ given a tolerance of ±0.1, which is recommended by Gleason et al. (2014). Also, we use [*lowerboundary_inte*, *upperboundary_inte*] as the threshold value of AMHG intercept, which is determined by $\log(w_c)/\log(Q_c)$ given a tolerance of ±0.1. Besides, we use the minimum and maximum value of discharge in priori knowledge as the threshold value of the discharge Q in AMHG, with name of [*lowerboundary_Q*, *upperboundary_Q*]. Then, function was fitted between the discharge in priori knowledge and the river width based on Eq. 1 ($w = aQ^b$), the coefficients were calculated as a and b. The calculated a and b values were used as a basis to construct a ± 50% interval (median method), and thus the thresholds is generated for a and b, which are [*lowerboundary_a*, *upperboundary_a*] and [*lowerboundary_b*, *upperboundary_b*].

3.2.4. Sensitivity tests and error assessment

To extend the application of the AMHG from large rivers to medium-to-small rivers, it is necessary to re-perform sensitivity analysis of the parameters (Fig. 4) to determine the key parameters that affect the AMHG mostly. There are AMHG slope, AMHG intercept, Q, a, b all 5 parameters in width-AMHG, in order to use GA to drive AMHG, the boundary of the parameter will be used as parameter in method. Specifically, *lowerboundary_b*, *upperboundary_b* represent lower boundary and higher boundary of b; *lowerboundary_a*, *upperboundary_a* represent the lower boundary and higher boundary of a; *lowerboundary_Q*, *upperboundary_Q* represent the lower boundary and higher boundary of Q; *lowerboundary_inte*, *upperboundary_inte* represent the lower boundary and higher boundary of AMHG intercept; *lowerboundary_slope*, *upperboundary_slope* represent the lower boundary and higher boundary of AMHG slope. The impact of a certain parameter on the accuracy (the RMSE) of the AMHG was investigated by increasing or decreasing the parameter value while keeping the other parameters constant.

The error assessment of estimation in this paper is not only by using RMSE (Eq. (5)) but also taking Nash–Sutcliffe efficiency (defined by Nash and Sutcliffe, 1970) into consideration.

$$\mathrm{NSE} = 1 - \frac{\sum_{t=1}^{T}\left(Q_o^t - Q_m^t\right)^2}{\sum_{t=1}^{T}\left(Q_o^t - \overline{Q}\right)^2} \tag{11}$$

where T is number of discharge observation, Q_o^t represent the observation value of discharge, $\overline{Q}$ is the average value of observation discharge, Q_m^t represent the estimation value of discharge.

4. Results

Parameter sensitivity analysis was initially used to screen the key parameters of the AMHG to improve the efficiency of the parameter calibration. Then initial values of the sensitive parameters at data-scarce stations were determined based on ground measurement at a reference station. Afterwards, the sensitive parameters were calibrated to facilitate estimation of streamflow by using AMHG. Subsequently, the accuracy of the AMHG in the estimation of the discharge of medium-to-small rivers was analyzed under two scenarios, i.e. the availability and unavailability of priori knowledge, was evaluated.

Taking the above-discussed as basis, the VHR-AMHG method was used to calculate the streamflow of medium-to-small rivers, and the calculation accuracy of this method was compared to that of the global–AMHG. The accuracy analysis was performed using Nash-Sutcliffe efficiency coefficient (NSE), RMSE and *t*-test, the null hypothesis of the t-test is that the average of estimation discharge is equal to ground-measured-discharge.

4.1. Parameter sensitivity analysis

To extend the application of the AMHG from large rivers to medium-to-small rivers, it is necessary to re-perform sensitivity analysis of the parameters (Fig. 4) to determine the key parameters that affect the AMHG mostly. There are AMHG slope, AMHG intercept, Q, a, b all 5 parameters in width-AMHG, in order to use GA to drive AMHG, the boundary of the parameter will be used as parameter in method. Specifically,

lowerboundary_b, *upperboundary_b* represent lower boundary and higher boundary of b; *lowerboundary_a*, *upperboundary_a* represent the lower boundary and higher boundary of a; *lowerboundary_Q*, *upperboundary_Q* represent the lower boundary and higher boundary of Q; *lowerboundary_inte*, *upperboundary_inte* represent the lower boundary and higher boundary of AMHG intercept; *lowerboundary_slope*, *upperboundary_slope* represent the lower boundary and higher boundary of AMHG slope. In the analysis, the global parameters were set as the reference and the RMSE was set as the target. The impact of a certain parameter on the accuracy (or RMSE) of the AMHG was investigated by increasing or decreasing the parameter value while keeping the other parameters constant. The percentage changes in the RMSE caused by the variations in the AMHG parameters are shown in Fig. 4.

As shown in Fig. 4(a)–(f), *lowerboundary_Q*, *upperboundary_Q*, *lowerboundary_a*, *upperboundary_a*, *lowerboundary_b*, and *upperboundary_b* have a large impact on the discharge estimation of medium-to-small rivers using the AMHG method resulting in >20% change in the RMSE, while the variation in the other parameters results in <10% change in the RMSE. Specifically, for *upperboundary_Q* and *lowerboundary_b*, a decrease in the parameter value (−%) significantly impacts the calculation result. When the parameter value changed from −10% to −50%, the RMSE rapidly increased, with the RMSE changing from +11% to +98% with the variation in *upperboundary_Q* and from +7% to +13% with the variation in *lowerboundary_b* (Fig. 4(a)–(c)). In contrast, the increase in the value of *lowerboundary_a* (+%) significantly impacted the calculation result. When the value of *lowerboundary_a* changed from +10% to +50%, the RMSE increased from +9% to +56% (Fig. 4(d)–(f)). For *upperboundary_a*, *lowerboundary_Q*, and *upperboundary_b*, an increase or decrease in the parameter value had a great impact on the calculation result. When the values of *upperboundary_a*, *lowerboundary_Q*, and *upperboundary_b* separately changed from +10% to +50%, the RMSE increased from +14% to +60%, +5% to +24%, and +5% to +15%, respectively. When the values of the three parameters were respectively changed from −10% to −50%, the RSME increased from +8% to +81%, +5% to +31%, and +3% to +21%, respectively (Fig. 4(a)–(f)). According to Gleason et al. (2014), by inputting different discharge information (i.e. *lowerboundary_Q* and *upperboundary_Q* values) for the sensitivity analysis of the AMHG method, it was found that different discharge thresholds (*lowerboundary_Q*, *upperboundary_Q*) for large rivers had a large impact on the results. In addition, it was observed that the thresholds of a and b (*lowerboundary_a*, *upperboundary_a*, *lowerboundary_b*, *upperboundary_b*) affected the accuracy of the estimated discharge, which is consistent with the results of this study. Therefore, it can be deduced that the key parameters affecting the AMHG calculation results include the six aforementioned parameters regardless of the size of the river. As such, further calculations were focused on these parameters.

4.2. Determination of initial values of the sensitive parameters at data-scarce stations based on ground measurement at a reference station

Based on the results of the parameter sensitivity analysis, rich historical data (priori knowledge) should be used to determine the initial values of the AMHG parameters *lowerboundary_Q* and *upperboundary_Q*, while Eq. (1) should be incorporated to determine the initial values of the other parameters *lowerboundary_a*, *upperboundary_a*, *lowerboundary_b*, and *upperboundary_b*. However, this is difficult to achieve in medium-to-small rivers where data are insufficient. Therefore, the Manning Equation coupled with ground-measured cross-section data were used to calculate discharge in areas that lack of data to act as a priori knowledge, A and P were calculated from cross-sections, while roughness n and the gradient S were obtained using UAV orthophotographs and the DSM. In particular, the roughness n required visual interpretation: from high-resolution UAV images, the vegetation on both river banks, slope protection conditions, soil type, and water surface width were identified and subsequently the roughness was determined using the roughness table as a reference (e.g., Sun, 2007); the gradient S was generated by calculating the relief between two water levels, one 300 m upstream from the cross-section and the other 300 m downstream. Therefore, the initial values of the six parameters can be determined using the river widths measured via UAV imagery.

To ensure the accuracy of parameter calibration after replacing ground-measured discharge with discharge calculated by the Manning Equation, an evaluation of the accuracy of the Manning Equation in calculating discharge was first performed using the rich historical discharge data of the WLT section and the cross-section data acquired from the WLT hydrological stations in the study area (Fig. 5a).

As shown in Fig. 5a, the ground-measured discharge and the estimated discharge from the Manning Equation are basically distributed along the 1:1 line (thin solid line), but most of the points are above it. The slope of the fitted linear curve is >1 (dashed line), indicating that the values estimated by the Manning Equation are slightly lower. The calculated NSE, RMSE and average relative error were 0.91, 7.08 m^3/s and 11.25%, respectively. The *t*-test yielded a P value > 0.05, meaning that although errors existed between the discharge values estimated by the Manning Equation and the ground-measured discharge values, the differences were not statistically significant; therefore, the values estimated using the Manning Equation can be used as historical data when the latter is absent. The Manning Equation was used to estimate the full tank discharge of 311.60 m^3/s, which was set as the AMHG parameter *upperboundary_Q*, while the dry streamflow value 0 was set as the value for *lowerboundary_Q*, i.e. [*lowerboundary_Q*, *upperboundary_Q*] = [0, 311.60].

After obtaining the discharge information using the Manning Equation, the corresponding river width information was extracted based on the ground-measured cross-sections, and the function was fitted between the discharge and the river width based on Eq. (1) (Fig. 5b). The coefficients were calculated as a = 21.102 and b = 0.2455 (Fig. 5b). However, the aforementioned calculated values were only station-specific parameters at one cross-section. To obtain the river-specific AMHG parameters, the calculated a and b values were used as a basis to construct a ± 50% interval (median method), and thus the thresholds for a and b were [*lowerboundary_a*, *upperboundary_a*] = [10.551, 31.653] and [*lowerboundary_b*, *upperboundary_b*] = [0.1228, 0.3682]. Using the above-determined values of the six parameters (*lowerboundary_Q*, *upperboundary_Q*, *lowerboundary_a*, *upperboundary_a*, *lowerboundary_b*, *upperboundary_b*), the optimal values of a and b could be obtained using the GA, and the discharge value at the calculation time could be further obtained using the AMHG.

In summary, using the Manning Equation and the ground-measured cross-section data to calculate the discharge results in a high accuracy, and the calculated values can act as historical data (a priori knowledge) for medium-to-small rivers that lack such data, so as to provide the AMHG with the initial values of the six key parameters: *lowerboundary_Q*, *upperboundary_Q*, *lowerboundary_a*, *upperboundary_a*, *lowerboundary_b*, and *upperboundary_b*.

4.3. Sensitive parameter calibration

After determining the threshold values of the aforementioned six key parameters, the optimal the value of a and b were calculated from Eq. (4) as follows. Given a selected cross section, the search space is defined by Section 3.2.3. The GA was used to determine the optimal value of a and b, thus minimizing the discharge difference for each section (Gleason et al., 2014).

To ensure the reliability of the results and achieve a high calculation speed, the number of iterations of the GA was set as 10 (Gleason et al., 2014). During the 10 simulations, based on the elitist selection strategy, the RMSE was used as the error indicator for the elimination of

individuals with excessively high error and retention of more adaptive individuals for the next population evolution.

Because population initialization in the GA is random, the parameters satisfying the requirements that the discharge difference in each section is the smallest may not be generated. With a higher number of population evolutions, there is a greater possibility for that, i.e. the RMSE approaches the optimal value as the number of generations increases (Holland, 1992; Karimkashi and Kishk, 2010). Therefore, in theory, it is better to have as many evolutions as possible. However, in reality, it is necessary to find a balance between the accuracy of the results and the efficiency of the execution. To determine the point of balance, the relationship curve between the RMSE and the number of generations was plotted (Fig. 6).

As shown in Fig. 6, the RMSE became relatively stable after 200 evolutions during each iteration, and an increase in the number of evolutions after 200 had a limited effect on the RMSE reduction. Therefore, in the subsequent calculations, the number of generations was set as 200 to effectively and accurately determine the AMHG parameters. In this way, sensitive AMHG parameters for all study rivers were calibrated. The results of [a,b] are respectively [13.13,0.29] for WLT, [34.75,0.13] for BDK, [5.90,0.39] for BDSH, [32.19,0.13] for CT, [9.03,0.34] for LJB, [52.16,0.15] for LCQ, [92.07,0.13] for LK,[5.28,0.23] for ZGNL, [18.45,0.19] for ZK. The optimized values of the parameters varied greatly with rivers.

4.4. Accuracy of streamflow inversion using the AMHG method at the reference station and in all medium-to-small rivers

As discussed in Gleason and Wang (2015), the AMHG leads to successful discharge estimation if the congruent discharge (Q_c) is within the range of previously observed discharge. Hence, before calculating streamflow using the AMHG method, a $Q_c = 8.31$ m^3/s calculated from −1/AMHG slope must fall within the range of [*lowerboundary_Q*, *upperboundary_Q*] (=[0, 311.60]) mentioned in Section 4.1 to ensure a high accuracy for the discharge estimation.

The GA is prone to premature convergence, i.e. convergence to a local optimal solution (Leung et al., 1997; Pandey et al., 2014). To ensure that the solution generated by the GA was the global optimal solution, 10 simulations were performed for each station using GA-driven AMHG (shown as the thin red line in Fig. 7), and the average value was used as the discharge estimation result (shown as the thick green line in Fig. 7). Under Scenario 1, the initial values of the parameters were determined using a priori knowledge for the subsequent discharge calculation using the AMHG. To quantitatively evaluate the accuracy of the AMHG calculations under the two scenarios, the WLT section, which had abundant ground-measured discharge and cross-section data, was selected for the experiment. The results are shown in Fig. 7.

As shown in Fig. 7, high and low ground-measured discharge values (gray circles) occurred as a result of field measurement error, but the values basically coincided with the discharge calculated by the Manning Equation (thick blue line). Compared to the ground measurements, the Manning Equation could prolong the discharge series; therefore, the discharge calculated using the Manning Equation was first used to verify the AMHG accuracy. Under Scenario 1, the AMHG-based simulated discharge and that calculated using the Manning Equation share the same trendline (the thick blue line in Fig. 7), with small errors occurring at mid-to-high values and large errors occurring at low values. The calculated NSE and RMSE were 0.94 and 5.12 m^3/s, respectively. Based on the *t*-test, $P = 0.73 > 0.05$, implying that there were no statistically significant differences between the results calculated using the AMHG and those calculated using the Manning Equation.

In areas where a priori knowledge is absent, the global parameters (Gleason et al., 2014) involved under Scenario 2 can be used to form the global–AMHG method to calculate the streamflow. The results are shown in Fig. 7 (10 simulation results [the thin red line] and 10 simulation evaluations [the thick black line]). Among the global parameters, *lowerboundary_Q* was calculated assuming a minimum 0.5-m/s flow velocity and 0.5-m river depth multiplied by the minimum observed width, whereas *upperboundary_Q* was similarly calculated using a 5-m/s flow velocity and 10-m river depth (Gleason et al., 2014). As a result, *lowerboundary_Q* = 9.21 m^3/s and *upperboundary_Q* = 4637.82 m^3/s. As the Q_c value did not fall between these two values in the WLT section, the AMHG calculation requirement was not satisfied.

As shown in Fig. 7 and from further analysis of Scenario 2, the NSE and RMSE of the discharge estimated using the AMHG and the Manning Equation were −201.16 and 313.32 m^3/s, respectively, indicating that the global parameters were not applicable in this section. The estimated discharge was significantly higher compared to the discharge calculated using the Manning Equation. Based on the *t*-test, $P = 0 < 0.05$, indicating a highly significant difference between the results of the two methods; therefore, the global parameters could not be applied to this section.

To perform an in-depth evaluation of the error, the results of the AMHG method under these two scenarios were further verified using ground-measured data, as shown in Fig. 8.

As shown in Fig. 8, Scenario 1 had an NSE of 0.88, an RMSE of 8.38 m^3/s, and an average relative error of 15.99% for all data. Therefore, the AMHG had high accuracy and can be applied. However, it cannot be used when there is a lack of cross-section data. Scenario 2 had an NSE of −161.54, an RMSE of 310.23 m^3/s, and $P = 0.00 < 0.05$, meaning that the calculation accuracy of the global-AMHG in the WLT section was low. Here we also respectively discussed discharges in dry and wet periods to evaluate errors: in dry season, scenario 1 had an RMSE of 15.27 m^3/s and scenario 1 had an RMSE of 226.04 m^3/s; while in wet season, scenario 1 had an RMSE of 24.25 m^3/s and scenario 1 had an RMSE of 403.82 m^3/s, indicating that AMHG perform better in dry season.

Relatively speaking, because Scenario 1 is highly dependent on historical data, the global–AMHG (scenario 2) is more likely to be used in medium-to-small rivers where historical data (cross-section and discharge) is scarce. However, global–AMHG has low calculation accuracy, as shown by the application in the WLT section. To further verify its capability of discharge inversion for medium-to-small rivers in the study area, eight representative stations were selected from Table 2 (Stations LCQ and LK did not meet the Q_c requirement, while stations BDSH, LJB, ZGNL, CT, BDK, and ZK met the requirement) (Fig. 1). The single-time ground-measured discharge data of these stations were used for further error analysis of the global parameters. The analysis results are shown in Table 3 and Fig. 9.

As shown in Fig. 9 and Table 3, the estimation accuracy for medium-to-small rivers using the global parameters was poor, with the RMSE and average absolute discharge error of each station being 332.64 m^3/s and 234.37 m^3/s, respectively.

In summary, from the calculation results for the medium-to-small rivers under both Scenarios 1 and 2, the parameters determined from the discharge calculated using the Manning Equation and the ground-measured cross-section (which acted as a priori knowledge (discharge information)) were more reliable than those obtained using the global parameters. Nonetheless, for medium-to-small rivers in which hydrological data (flow, cross-sections, etc.) is often absent, the use of global parameters in calculating discharge is more advantageous as it does not require a priori knowledge. However, the low accuracy of the global–AMHG method makes its application to data-scarce areas problematic; therefore, there is an urgent need for new methods to solve this problem.

4.5. Streamflow calculation using the VHR-AMHG method and its accuracy

The VHR-AMHG method proposed in this study effectively incorporates the advantages of Scenario 1, and can replace the global–AMHG in estimating the discharge in data-scarce areas. To achieve this purpose, reasonable initial values must be set for the six most sensitive key parameters (*lowerboundary_Q*, *upperboundary_Q*, *lowerboundary_a*,

Table 3
Medium-to-small streamflow estimation using the global parameters.

Station	Ground-measured discharge (m^3/s)	Global-AMHG discharge (m^3/s)	Absolute error (m^3/s)
BDK	5.37	215.31	209.94
BDSH	2.37	5.84	3.47
LK	263.00	956.85	693.85
ZGNL	1.14	132.24	131.10
LJB	3.93	39.51	35.58
LCQ	33.93	485.10	451.18
ZK	0.31	268.23	267.92
CT	2.73	139.30	136.57

upperboundary_a, *lowerboundary_b*, and *upperboundary_b*) discussed in Section 4.1 to improve the accuracy of the AMHG method. As historical hydrological data is needed but such data is usually unavailable for medium-to-small rivers, the proposed solution is as follows: First, the measured sections of the WLT were categorized into VirtualP and RealP as shown in Fig. 3(a), then Q_1 and Q' were calculated using Eq. (6) and the relationship was fitted to a linear equation based on Eq. (7). The resulting equation was $Q' = 1.65Q + 23.94$ ($R^2 = 0.99$, RMSE $= 4.08\ m^3/s$). Second, using associating river width data at the WLT station with that of the other stations, the river width ratio (WRatio) was calculated using Eq. (8). Following Eq. (9), the Q and Q' expressions of all stations (including the reference station WLT) were calculated as shown in Table 4. Thus, for any river in the study area,

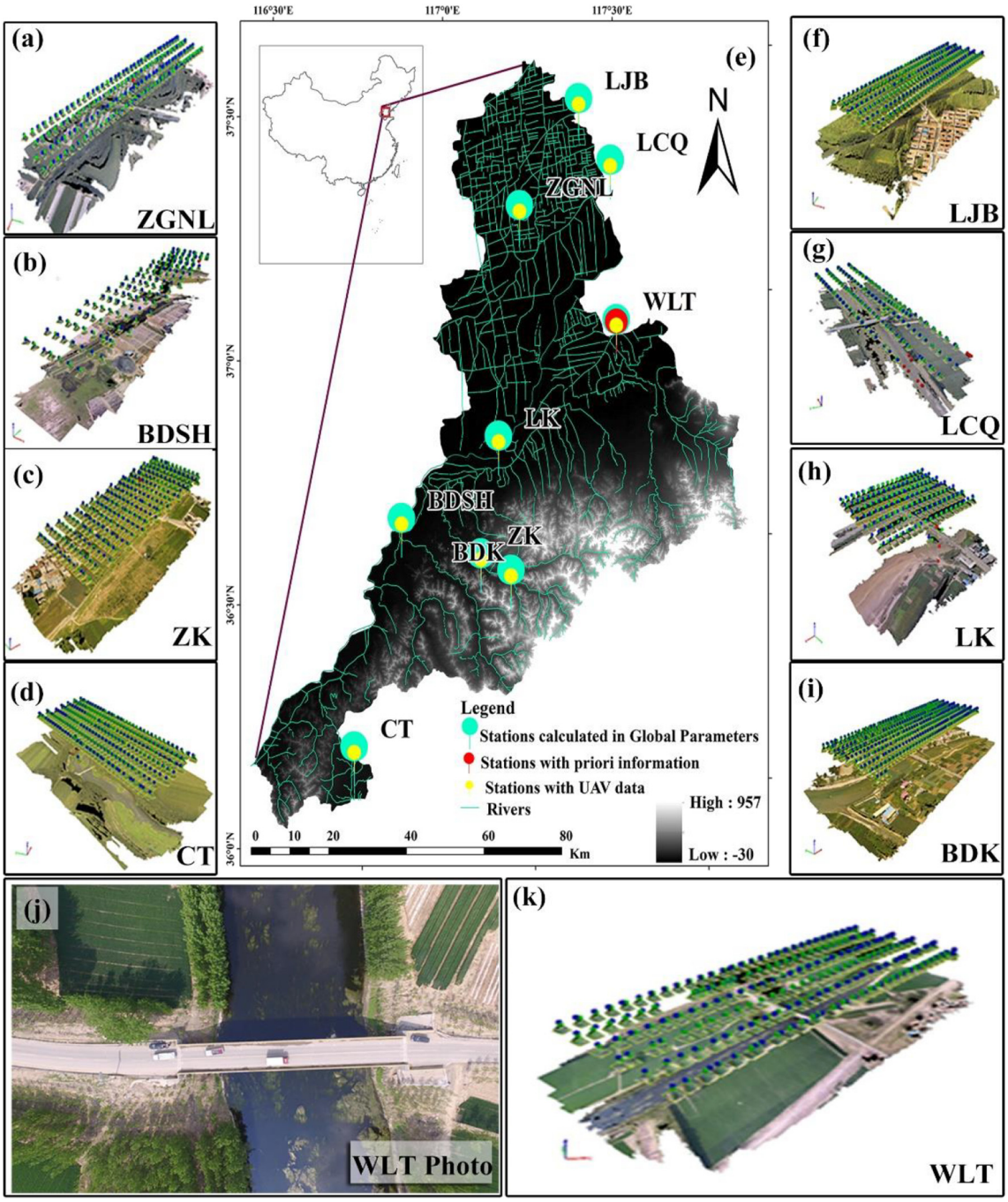

Fig. 1. Study area and the representative monitoring stations: (a)–(d), (f)–(i), and (k) represent the generated digital surface model (DSM) and point cloud using UAV imagery; (e) shows the locations of the representative monitoring stations; and (j) is an aerial photo corresponding to k via UAV.

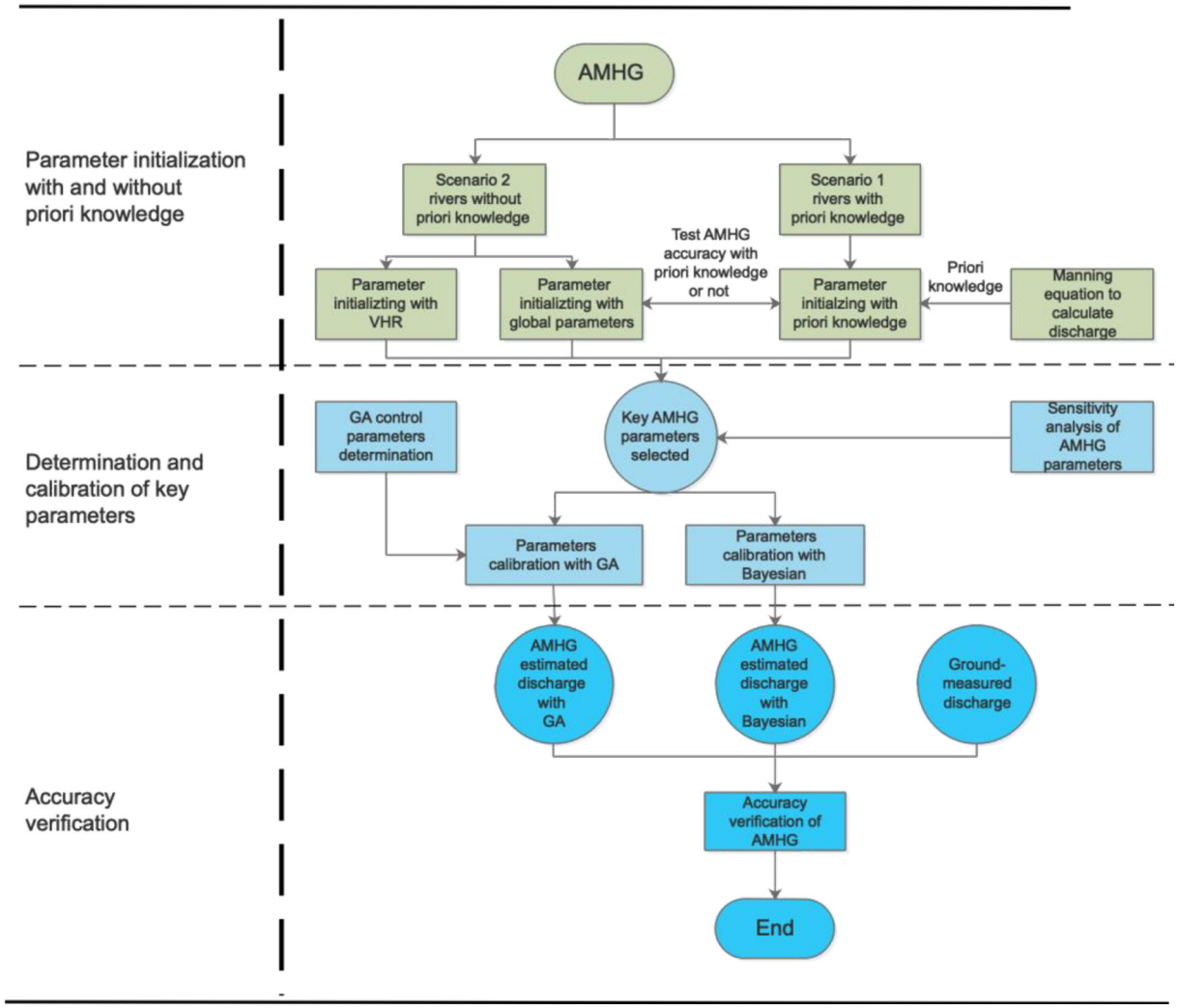

Fig. 2. Technology roadmap designed to verify AMHG.

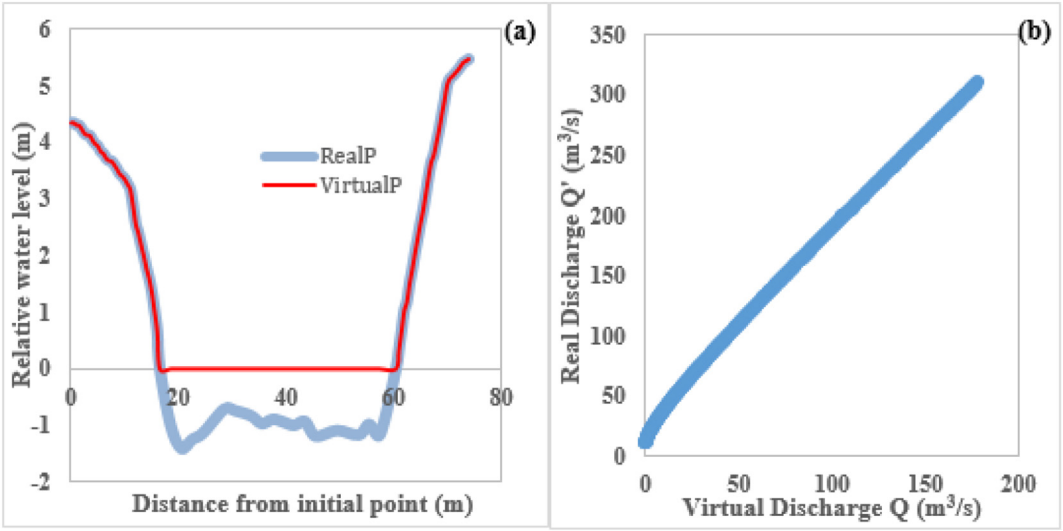

Fig. 3. VHR method and the Q-Q′ relationship curve. (a) VHR diagram, in which the y axis is the relative elevation with the water surface as a reference; (b) scatter plot of the virtual discharge (Q) and real discharge (Q′) both calculated from the Manning Equation at different water levels according to VirtualP and RealP in panel a. A strong linear relationship exists between Q and Q′.

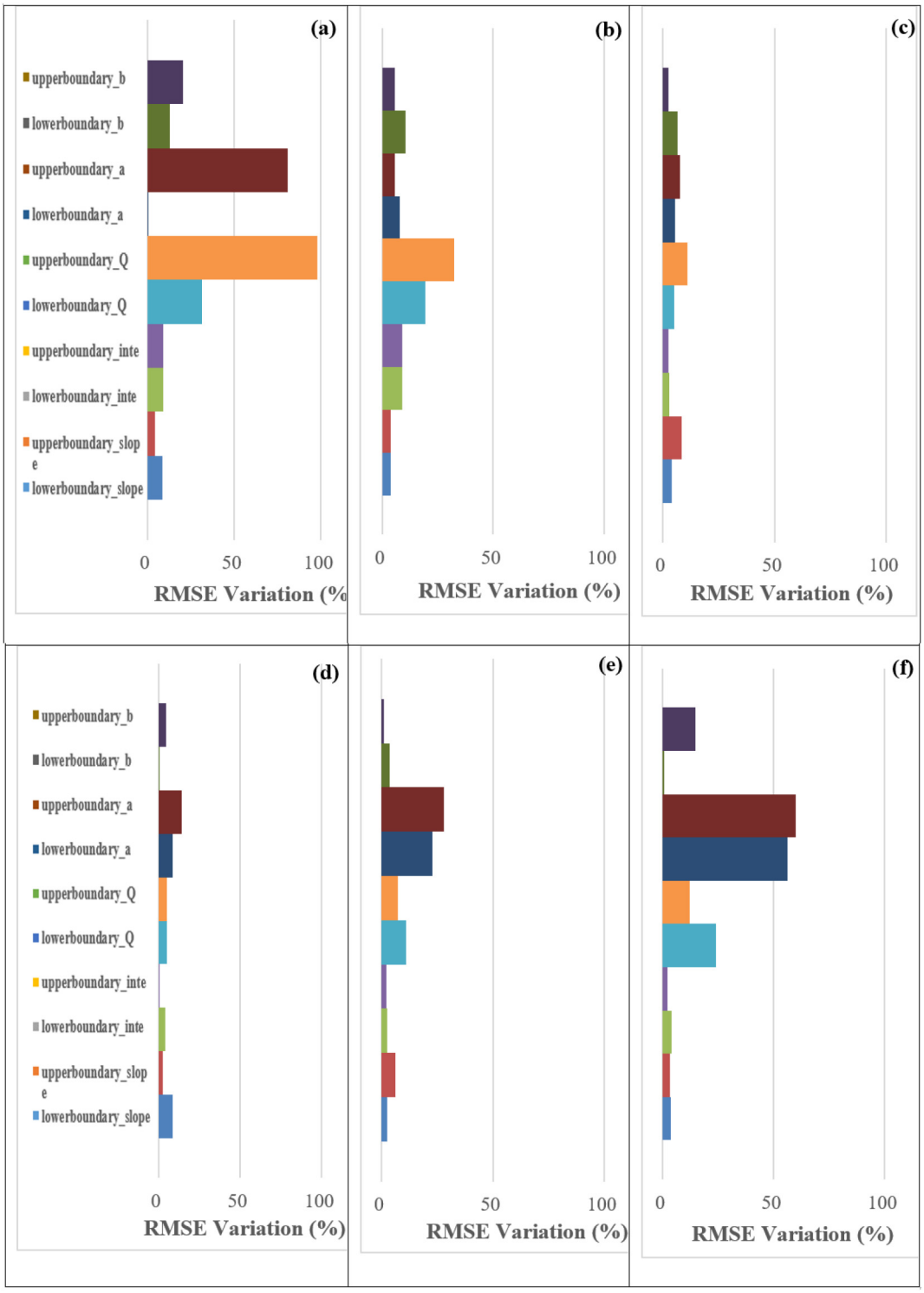

Fig. 4. Sensitivity analysis of parameters. Each subgraph represents the percentage change in the RMSE caused by the variation in each AMHG parameter as follows: (a) −50%, (b) −20%, (c) −10%, (d) 10%, (e) 20%, and (f) 50%. *upperboundary_b*, *lowerboundary_b*, *upperboundary_a*, *lowerboundary_a*, *upperboundary_Q*, *lowerboundary_Q*, *upperboundary_inte*, *lowerboundary_inte*, *lowerboundary_slope* and *upperboundary_slope* represent the AMHG parameters.

the real discharge could be obtained using the WRatio correction based on the Q and Q′ expressions fitted using the data of the WLT station. Eventually, the goal of generating the initial values for the AMHG parameters without using any historical hydrological data (discharge and cross-sections) was achieved.

In practice, at each station in the study area (Table 2), the initial values of the six key parameters were determined with the VHR-estimated discharge data. With these limited values, AMHG was then used to calculate streamflow at each station. It must be noted that the VHR-estimated discharges have biases due to the unknown of actual cross-sections and can solely be used to calculate AMHG-parameter initial values. The biases were eliminated in the AMHG-calculated discharges since the parameters with the initial values were further optimized by using the GA, and the discharge data were generated from the AMHG calculations. The initial values of the six parameters of each station are shown in Table 5.

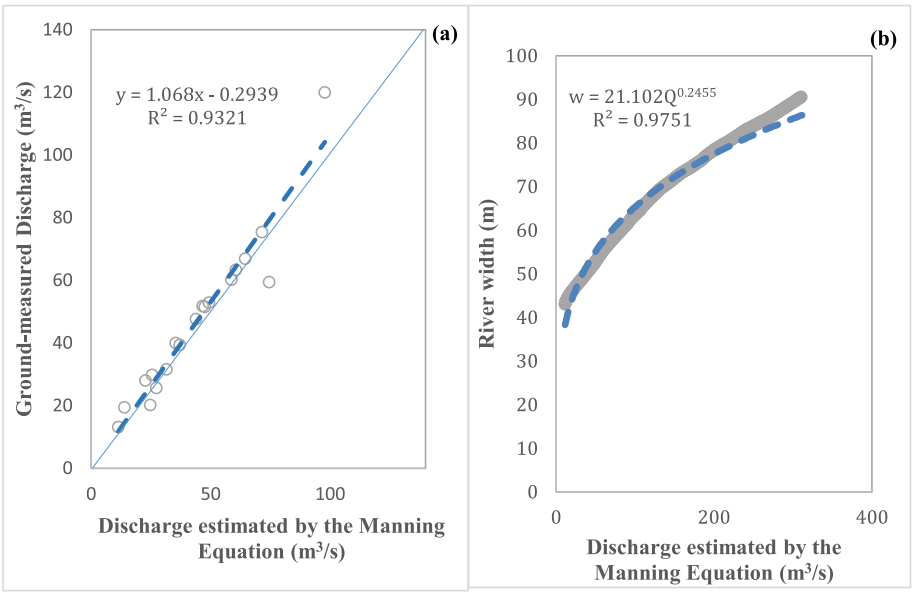

Fig. 5. Relationships between the discharge estimated by the Manning Equation and (a) ground-measured discharge and (b) UAV-measured river width. The thin solid line represents the 1:1 line, while the dotted line represents the trend line.

Before using the VHR-AMHG method to calculate the discharge, Q_c must fall within the [*lowerboundary_Q, upperboundary_Q*] interval of the VHR. Results indicated that nine rivers did not satisfy this condition (Fig. 10). Under such circumstances, to evaluate the accuracy of the VHR-AMHG, the six key parameters generated using the VHR and the global parameters were, respectively, input into the AMHG for calculation and compared to the ground-measured values as shown in Fig. 9.

As shown in Fig. 9, the VHR-AMHG (Red) was more suitable for the estimation of medium-to-small streamflow. The RMSE between the estimation and ground measurement (dark blue) was 32.15 m^3/s, while the average error was 24.06 m^3/s. However, the RMSE between the discharge estimated using global–AMHG (gray dotted line) and the ground measurement was 301.80 m^3/s, while the average error was 220.33 m^3/s. Moreover, the results at each station were unstable compared to the ground measurement values (dark blue). In conclusion, the VHR-AMHG method (Eqs. (7)–(9)) proposed in the present study is suitable for discharge calculation, as it generate parameters that can effectively replace the global parameters for medium-to-small rivers with scarce data when Q_c does not satisfy the requirement. Although uncertainties still exist in the VHR-AMHG results, a significant enhancement in calculation accuracy was still achieved.

5. Discussion

5.1. Calculation of discharge using the Manning Equation

For medium-to-small rivers with scarce data, the discharge calculated using the Manning Equation provides the initial values for the AMHG parameters. The Manning Equation has been widely used in discharge calculations (Vatankhah et al., 2015). It relies mainly on parameters such as water depth (or water level), water surface width (or water area), water surface velocity, and water surface gradient (Song et al., 2011). LeFavour and Alsdorf (2005) estimated the streamflow of three locations on the Amazon River based on the Manning Equation, and found that the error was within 8% compared to the measured data. Voinov et al. (1999) used the Manning Equation in a landscape

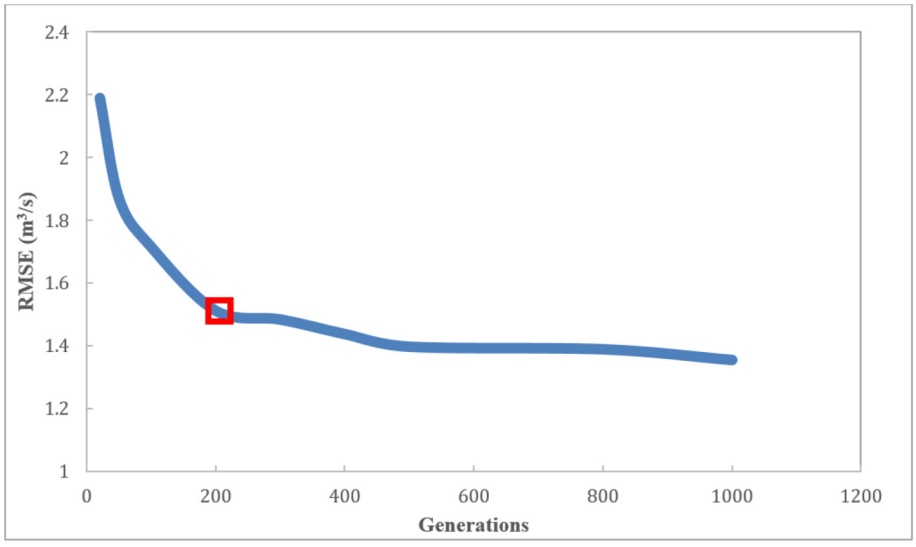

Fig. 6. Variation in the RMSE during the evolutionary process of the GA. The red box represents the mutation point, after which the RMSE became relatively stable. (For interpretation of the references to color in this figure legend, the reader is referred to the web version of this article.)

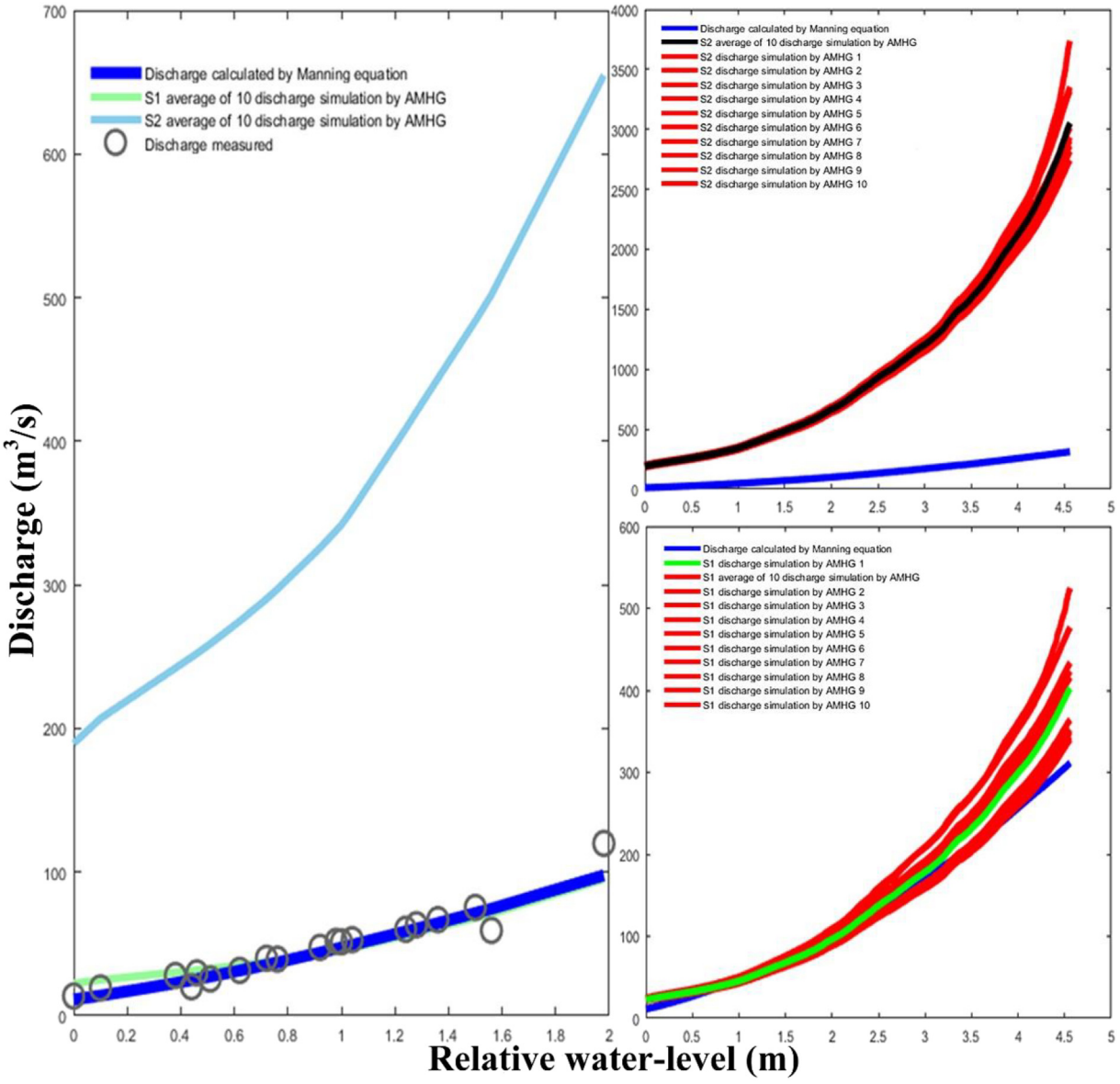

Fig. 7. Medium-to-small river discharge calculated using the AMHG under two scenarios. Scenario 1 (S1) represents the AMHG-estimated discharge driven by the Manning Equation and ground-measured cross-section parameters. Scenario 2 (S2) represents the AMHG-estimated discharge driven by the global parameters by Gleason et al. (2014). The relative water level was measured based on the water surface when the UAV flew.

ecological model to calculate water flux in southern Florida; Westerberg and Hagberg (2018) applied the Manning Equation to obtain a conservative estimate of the maximum discharge in the bedrock-controlled upper part of the Engaruka River; and Pan et al. (2016) established river stage-discharge rating curves in the Illinois River through the combined use of the Manning Equation and remote-sensing data.

From the present study, it was found that the discharge values estimated using the Manning Equation were slightly less than the ground measurements. This is consistent with results obtained by other studies. There are two main reasons for this phenomenon: (1) The roughness value has an important impact on the estimation. In rivers with gravel riverbeds, the roughness decreases as the water level increases, which explains why estimations based on the Manning Equation were lower (Lane, 2005; Dingman, 2009). In sand-bed reaches, the correlation between roughness and discharge is significantly positive; however, the correlation is significantly negative for gravel-bed pool-riffle reaches and small cobble/boulder cascade reaches (Ferguson, 2010). (2) The gradient and hydraulic radius indices have a significant influence on the results. When the Manning Equation is applied to natural rivers, the index of gradient S should be 0.33 instead of 0.5 (the S index is 0.5 in Eq. (6)) (Bjerklie et al., 2005); when applied to gravel-bed rivers and mountain streams, the index of the hydraulic radius (R in Eq. (6)) should be >0.66, and the index of the gradient S should also be within the interval [0.25,0.50] (López et al., 2007). The aforementioned studies have shown that the Manning Equation provides smaller estimated values of discharge when applied to natural rivers, which is consistent with the results of the present study. However, the results of the *t*-test indicated that the differences between the ground-measured discharge and discharge values estimated using the Manning Equation were statistically insignificant. Hence, it is feasible to use the Manning Equation to approximately estimate the initial values of the AMHG parameters.

5.2. GA parameter calibration

In the present study, the RMSE was used as the objective function for the calibration of the AMHG parameters with the GA. In GAs, the selected objective function usually has an important influence on calibration (Li et al., 2017; Srinivas and Patnaik, 1994). The selection of the

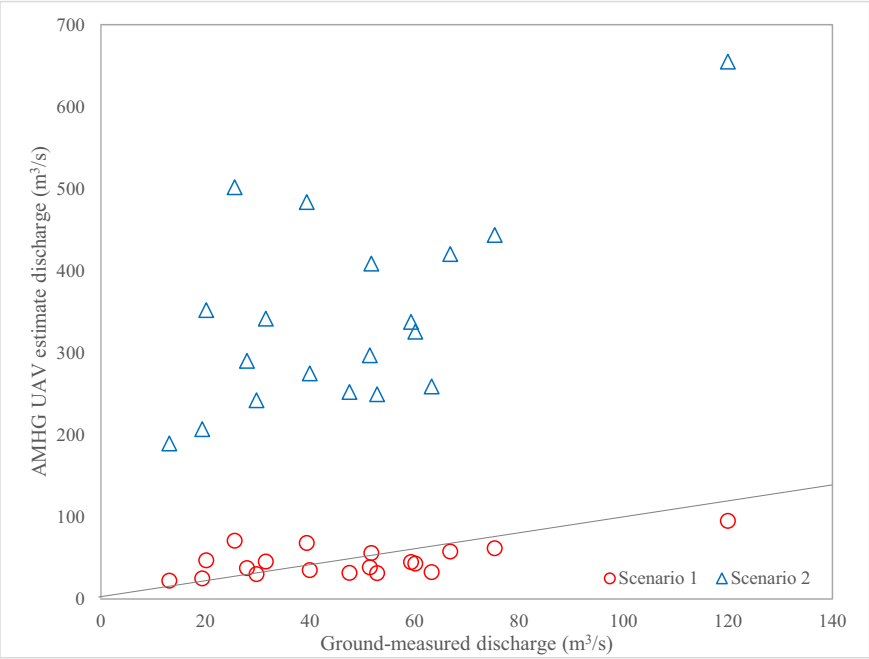

Fig. 8. Error analysis diagram of the AMHG-UAV estimated discharge; the gray line represents the 1:1 line.

objective function directly affects the convergence speed of the GA and determines whether the optimal solution can be achieved, as a GA does not utilize external information in the evolutionary search and is solely dependent on the objective function to perform the search based on the fitness of each individual in the population (Fei et al., 2017; Fonseca and Fleming, 1993). Time complexity is often used to describe an algorithm's use of computational resources. As complex objective functions increase the time complexity of GAs, researchers often use simple objective functions in the selection process of a GA algorithm to reduce time complexity (Fei et al., 2017; Konak et al., 2006; Nopiah et al., 2010). For this reason, the simple RMSE was used as the objective function in the present study. It is an indicator commonly used in genetic algorithms (Herman et al., 2018; Moriasi et al., 2007). For instance, Chlumecký et al. (2017) optimized the SAC-SMA model parameters using RMSE; Chadalawada et al. (2016) presented the dynamics of the urban rainfall-runoff process using RMSE and GAs (Chadalawada et al., 2016). Dhamge et al. (2012) used RMSE and GAs to calibrate parameters for artificial neural networks to estimate runoff. For complex hydrological models, multiple indicators such as NSE are often considered (Herman et al., 2018). In the present study, good results were achieved when both NSE and RMSE were used in accuracy evaluation.

5.3. Optimization of the calculation accuracy of the AMHG

The present study showed that the global–AMHG method is not stable for estimating the discharge of medium-to-small rivers, which is consistent with the results of other studies. In a study on the theoretical basis of AMHG, Gleason and Wang (2015) asserted that in the estimation of discharge using AMHG, realistic minimum and maximum discharge constraints for the specific study rivers should be considered. Durand et al. (2016) compared AMHG and other commonly used satellite estimation methods and found that calculations using the global parameters of AMHG performed much more poorly.

From the perspective of the initial value setting of parameters, as Gleason's global parameters were developed based on large rivers (average river width of 629 m) (Gleason et al., 2014), they possess a certain degree of universality but are not applicable to all rivers. As the data in

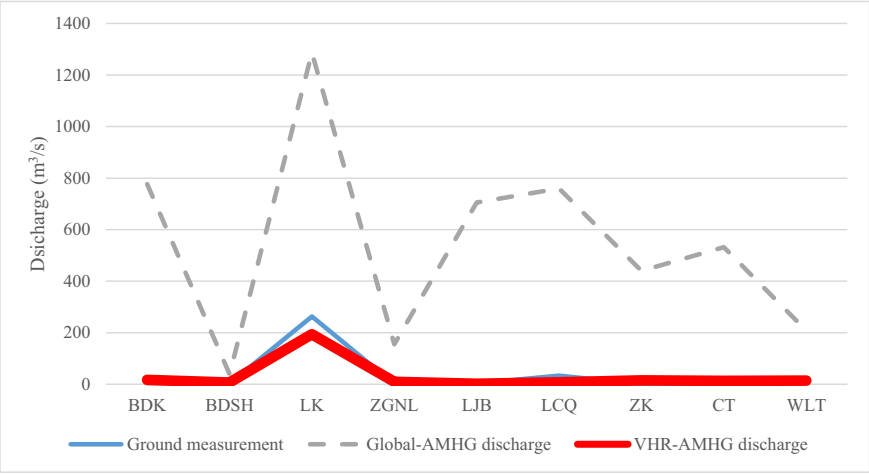

Fig. 9. Comparison of the AMHG-UAV estimated discharge for medium-to-small rivers.

Table 4
VHR expressions of all the rivers in the study area.

Station	Expression
BDSH	$Q' = 0.93 * Q + 13.50$
BDK	$Q' = 2.74 * Q + 39.93$
CT	$Q' = 2.06 * Q + 29.93$
LCQ	$Q' = 3.32 * Q + 48.30$
LJB	$Q' = 1.90 * Q + 27.67$
LK	$Q' = 8.24 * Q + 119.99$
WLT	$Q' = 1.65 * Q + 23.95$
ZK	$Q' = 2.22 * Q + 32.35$
ZGNL	$Q' = 0.92 * Q + 13.33$

the present study were acquired from medium-to-small rivers (average river width of 69 m), the parameters could not be directly used.

Considering the limitations of the AMHG, when applied to large rivers, the calculation results of low-b rivers (i.e. rivers with a lower b value derived from Eq. (1) based on discharge and river width) are not satisfactory. As the b value is related to the shape of the river channel (Gleason et al., 2014), there is a theoretical difference in the definition of low-b rivers for large rivers and for medium-to-small rivers. To investigate if the AMHG is inapplicable to medium-to-small rivers with a low b value, the difference between the threshold value of b between medium-to-small rivers and large rivers was analyzed. The b values of the stations in the study area are shown in Table 6.

According to Table 6, large absolute errors occurred during the estimation of the discharge of low-b rivers using AMHG. Gleason et al. (2014) reported that the application of AMHG to low-b ($b < 0.1$) rivers produced unsatisfactory results. Based on the calculations of the present study, the error significantly increased when $b < 0.25$; therefore, the low threshold value of b for medium-to-small rivers could be set as 0.25. Because of the different scales of the rivers studied, the conclusions arrived in the present study were similar but not entirely identical to those of Gleason et al. (2014). In short, regardless of the scale of the river, the low threshold b value is among the key factors that constrains the use of AMHG in calculating streamflow.

AMHG leads to successful discharge estimation if congruent discharge ($Q_c = -\frac{\Delta\ loga}{\Delta b}$) is within the range of observed discharge ($Q_{min} < Q_c < Q_{max}$) (Barber and Gleason, 2018). This is consistent with the calculation result achieved for the WLT section in the present study. However, in subsequent calculations, the use of VHR for the initial value setting of the parameters resulted in a higher accuracy than the use of global parameters, given that the Q_c value did not meet the requirement.

To fully explore the influence of the initial parameter value setting and the fulfilment/non-fulfilment of the Q_c requirement on the AMHG calculation result, the discharge of all rivers in the study area was calculated using two parameter value setting methods, i.e. the VHR and global parameters. The calculation errors of the two methods under

Table 5
VHG-generated parameters at each station.

Station	*lowerboundary_Q*	*upperboundary_Q*	*lowerboundary_a*	*upperboundary_a*	*lowerboundary_b*	*upperboundary_b*
BDSH	13.50	36.63	0.26	0.77	0.63	1.90
BDK	39.99	103.29	31.31	93.92	0.03	0.08
CT	29.99	216.00	25.57	76.72	0.04	0.11
LCQ	48.37	838.86	57.10	171.30	0.03	0.09
LJB	27.72	94.35	11.25	33.76	0.09	0.27
LK	123.62	612.18	106.53	319.58	0.01	0.03
WLT	23.96	316.91	9.07	27.21	0.14	0.41
ZK	32.42	309.55	14.84	44.52	0.08	0.24
ZGNL	13.34	22.40	6.40	19.21	0.08	0.24

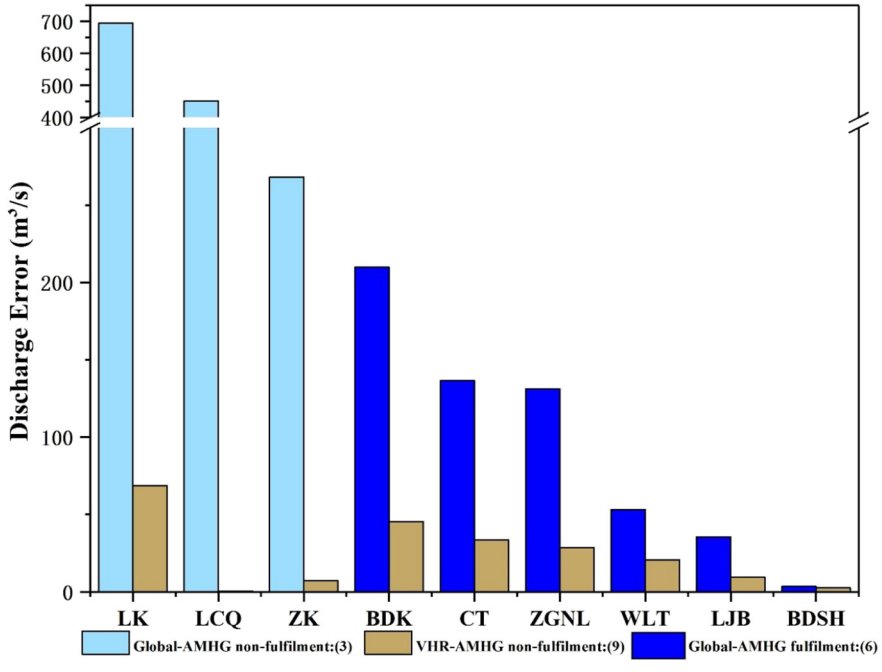

Fig. 10. Calculation errors under different parameter conditions, categorized according to the fulfilment/non-fulfilment of the discharge range by Q_c.

Table 6
Absolute error of estimated discharge and b value at each station.

Station	Absolute error of discharge (m^3/s)	b value
LK	68.74	0.03
CT	45.45	0.13
ZK	33.47	0.17
LCQ	28.48	0.07
BDK	20.70	0.22
LJB	9.54	0.39
WLT	7.17	0.28
ZGNL	2.51	0.93
BDSH	0.45	1.33

two scenarios, i.e. the fulfilment or non-fulfilment of the Q_c requirement, were subsequently analyzed. For the global–AMHG method, six rivers satisfied the condition that Q_c was within the range of discharge, while three rivers did not satisfy this condition. For the VHR-AMHG method, all nine rivers did not satisfy the requirement. When the global–AMHG method proposed by Gleason et al. (2014) was used to calculate Q_{min} and Q_{max} to define the discharge interval applicable to all stations, three out of the nine rivers of the study area did not satisfy the Q_c requirement. When the same calculations were performed using the VHR method, all nine rivers did not meet the requirement, which implies that the proposed method of the present study is more stringent compared to the global parameters.

Further analysis of the calculation errors for rivers under different conditions in the study area is shown in Fig. 10.

Fig. 10 shows that for the rivers having Q_c values that satisfy the requirement, the error of estimation using the global parameters was 130.77 m^3/s, while the error was 390.45 m^3/s for rivers that did not satisfy the requirement. This indicates that under the same parameter conditions, the AMHG has a higher accuracy for rivers that meet the requirement. However, parameter setting, or selection of VHR or global parameters, remains as the factor having the greatest influence on calculation accuracy. Although the parameters calculated using the VHR did not satisfy the requirement that "Q_c must be within the discharge

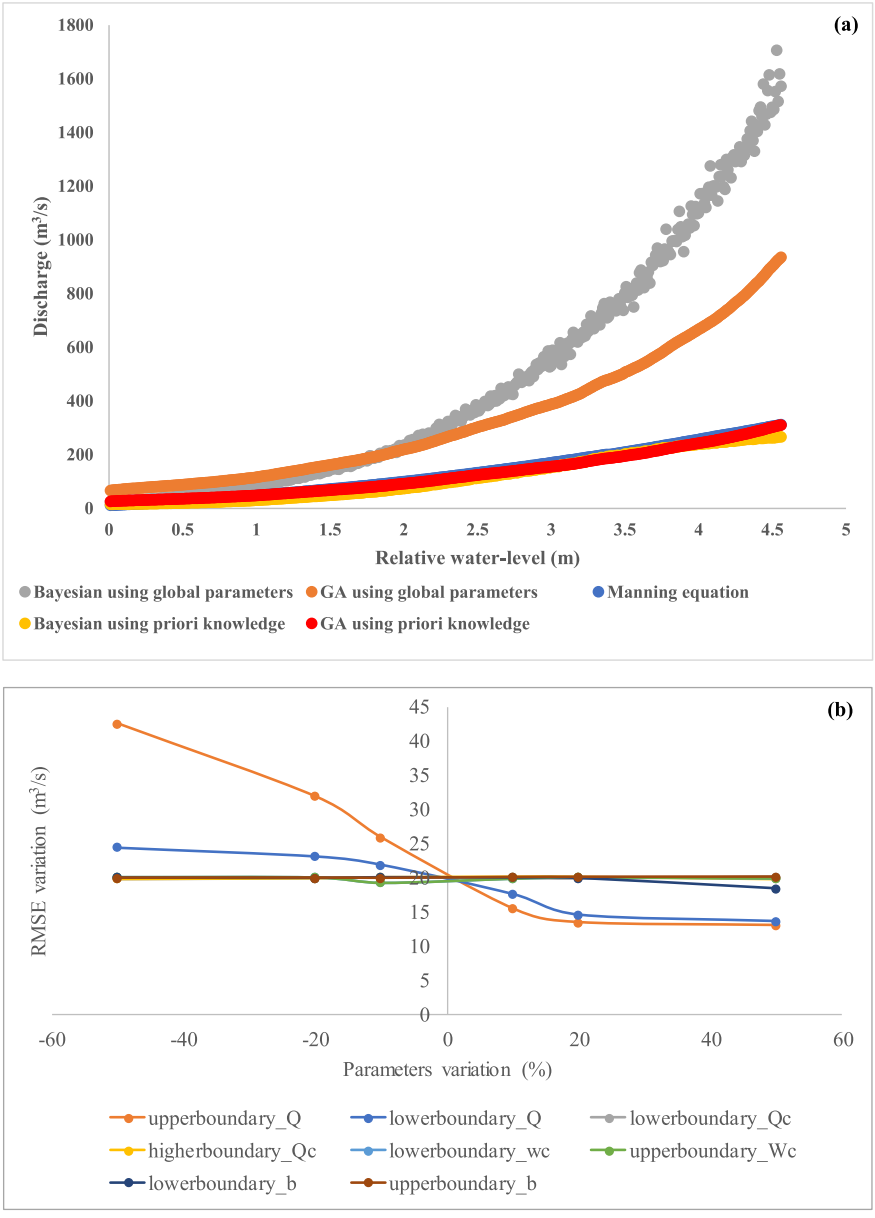

Fig. 11. Comparison of GA- and Bayesian-AMHG. (a) Comparison of GA- and Bayesian-AMHG calculated discharge with Manning equation calculated discharge. (b) Sensitivity analysis on Bayesian-AMHG parameters.

range," its error was much smaller than that of the global parameters method, which partly satisfied the Q_c requirement. This means that the VHR method proposed in the present study has eliminated the limitation of "Qc must be within the range of observed discharge" when using the AMHG, thereby expanding the scope of application of AMHG.

5.4. GA-AMHG vis-à-vis Bayesian-AMHG

Hagemann et al. (2017) used the Bayesian method instead of GA to provide optimized parameters for AMHG, and they concluded that the GA will give a more similar result to known flow than Bayesian method when passing priori knowledge, with low error metrics. To compare the performance of GA-AMHG with that of Bayesian-AMHG, WLT station was used to test the difference of the two methods, as shown in Fig. 11a.

While the discharges calculated with GA-AMHG using priori knowledge (red point in Fig. 11a, RMSE = 8.38 m^3/s) and with the Bayesian-AMHG using priori knowledge (yellow point, RMSE = 19.57 m^3/s) show very few differences with manning equation calculated discharge (blue point), those by GA-AMHG using global parameters (orange point, RMSE = 310.23 m^3/s) and by Bayesian-AMHG using global parameters (gray point, RMSE = 488.14 m^3/s) show quite large biases compared with manning equation results. For areas with abundant priori knowledge GA-AMHG using priori knowledge is recommended. Furthermore, Bayesian-AMHG increases RMSE from 72.86 m^3/s to 488.14 m^3/s when using global parameters, and increases RMSE from 8.38 m^3/s to 19.57 m^3/s when using priori knowledge. Consequently, GA-AMHG performs better than Bayesian-AMHG both when using priori knowledge and global parameters, which is consistent with Hagemann et al. (2017). In other words, AMHG based on either GA or Bayesian cannot perform well without priori knowledge. Our study, developed a new VHR method to provide priori knowledge for AMHG, undoubtedly enlarges the application extent of AMHG, especially for data-scarce areas. Besides, Bayesian methods require certain constraints in their unknown parameters which are imposed as 'prior' probability distributions (Hagemann et al., 2017; Zhang et al., 2009). Researchers often use historical information as Bayesian' prior: Hagemann et al. (2017) used priori knowledge (or known flows) for Bayesian to provide parameters for discharge calculation; Reis Jr and Stedinger (2005) used Bayesian methods, taking known flood records as priori knowledge, to evaluate the posterior distributions flood frequency; Parent and Bernier (2003) pointed out that only when a sample of historical data are available can Bayesian method be used to deal with the classical Poisson–Pareto peak over threshold (POT) model for discharge estimation.

To further discuss the indispensability of priori knowledge for an accurate calculation with AMHG, sensitivity analysis on Bayesian-AMHG parameters following Section 4.1 was conducted in Fig. 11b, showing that the orange line (*upperboundary_Q*) and the sky-blue line (*lowerboundary_Q*) vary the greatest. Combined with the conclusion in Section 4.1, the threshold of discharge always counts for AMHG, suggesting that precise priori knowledge is highly demanded in an accurate AMHG calculation. The above-discussed implies that the VHR method proposed in our study, although with a few error, is applicable to provide initial parameters for GA-AMHG, however, it is not appropriate for Bayesian-AMHG because Bayesian method has much higher requirement on priori knowledge (Parent and Bernier, 2003; Reis Jr and Stedinger, 2005). This certifies the feasibility and reasonability of combining VHR with GA-AMHG in our study.

5.5. Potential application of VHR-AMHG

The VHR-AMHG was developed based on UAVs imagery. However, there are some limitations with UAVs remote sensing technology. For instance, limitation on battery capacity will make UAVs can only collect data at a relatively short time which makes the obtained measurements instantaneous (Watts et al., 2012; Toth and Jóźków, 2016). Besides, UAV color camera system usually cannot work in the night or under weak illuminated condition (Woo et al., 2007; Wei et al., 2016). These greatly limit the application of traditional methods based on UAVs for streamflow retrieval, especially in remote (data-scarce) areas where the intra- and inter-annual variability of discharges is extreme large. In order to overcome these shortcomings of UAVs, the VHR-AMHG is designed to be able to calculate long series synthetic width and discharge of river by once flight, thus produces long-series synthetic width and discharge by once UAV flight whereby width-discharge curve can be fitted. After constructing long-series width-discharge curve, high-resolution satellite images, which can be obtained easily throughout a year, can be used as a data source to monitor the intra- and inter-annual variability of river width whereby to retrieve discharge if the studied river cross-section keeps stable. For example, the GeoEye-1 (with the spatial resolution of 0.41 m per pixel) (Choi et al., 2012; Ielpi, 2017), WorldView-4 (with the spatial resolution of 0.31 m per pixel) (Sozzi et al., 2018) and GF-2 (with the spatial resolution of 1 m per pixel) (Chu et al., 2016) could provide reliable river width values. Based on the width-discharge curve constructed with help of UAVs and river width values measured by using real-time satellite images, discharges in the daytime could be acquired. In the night time, the synthetic aperture radar satellite image can provide river width information to monitor discharge variation, such as TerraSAR-X (with the spatial resolution of 1 m per pixel) (Pitz and Miller, 2010; Shen et al., 2019), Alos-2 (with the spatial resolution of 1 m per pixel) (Kankaku et al., 2013), GF-3 (with the spatial resolution of 1 m per pixel) (Chen et al., 2017).

6. Conclusion

The present study evaluated the accuracy of the inversion of medium-to-small streamflow by investigating two different scenarios (with or without a priori knowledge) through the use of the AMHG method in combination with UAV remote sensing in data-scarce medium-to-small rivers in Jinan City. A VHR method was proposed to provide the initial values of the AMHG parameters for rivers with scarce data. The results of the study are as follows:

(1) For the reference station WLT, under the scenario where a priori knowledge was available, the NSE and RMSE were 0.88 and 8.38 m^3/s, respectively, and the method yielded high accuracy results thus making it applicable to the estimation of streamflow in WLT section. Under the scenario in which a priori knowledge was unavailable and the global parameters were used to calculate discharge, the NSE is −161.54, an RMSE is 310.23 m^3/s, respectively, and the method yielded low accuracy results making it unsuitable for calculating discharge on the section. Subsequently, discharge estimation using the global parameter-AMHG method was performed on other medium-to-small rivers in Jinan City that lacked a priori knowledge (discharge information). The resulting RMSE and average absolute error were 332.64 m^3/s and 234.37 m^3/s, respectively, proving that the global parameter-AMHG method is not suitable for discharge calculation of medium-to-small rivers with scarce data.

(2) When the proposed VHR-AMHG method was used to calculate discharge in data-scarce medium-to-small rivers in the study area, an RMSE of 32.15 m^3/s and an average absolute error of 24.06 m^3/s were obtained, which were superior to those of the global parameter-AMHG method and indicated a significant enhancement of calculation accuracy. Therefore, the proposed VHR-AMHG method expanded the application range of AMHG to rivers of all sizes.

(3) Regardless of the size of the river, the low threshold value of b is among the key factors that constrains the application of discharge estimation using the AMHG (Gleason et al., 2014; Barber et al., 2018). For large rivers, a low-b river is defined as $b < 0.1$ (Gleason et al., 2014), while for medium-to-small rivers, it is

defined as b < 0.25. The AMHG method is not recommended for low-b rivers.

(4) For rivers that satisfy the requirement that "congruent discharge (Q_c) must be within the range of discharge," the accuracy of the AMHG in discharge estimation is higher compared to that of rivers that do not satisfy the requirement. However, the accuracy of the initial values of model parameters has a greater impact on the accuracy of the AMHG calculations. In addition, results have shown that the novel VHR-AMHG method proposed in the present study effectively eliminates the limitation of the Q_c requirement.

(5) GA-AMHG performs better than Bayesian-AMHG both when using priori knowledge and global parameters. More importantly, AMHG based on either GA or Bayesian cannot perform well without priori knowledge. Our study developed a new VHR method to provide priori knowledge for AMHG, undoubtedly enlarges the application extent of AMHG, especially for data-scarce areas.

Overall, it is feasible to use the AMHG method to calculate the discharge of global medium-to-small rivers with proper initial value setting of the parameters. The VHR method proposed in the present study provides an alternative parameter-setting method for areas with scarce historical data, and improves the accuracy of the AMHG for discharge calculation in these areas.

Because of the impact of roughness and other indices (ratio and hydraulic radius), the estimated values calculated using the Manning Equation were lower than measured values, thus introducing a certain degree of uncertainty to the results of the present study. For future studies, the Manning Equation must be modified to improve the estimation accuracy. Additionally, the irregularity of cross-sections often resulted in great uncertainties especially in the estimation of small discharges, e.g., estimation of 1.14 m^3/s discharge with a relative error of 219% at ZGNL station. Future improved VHR with full consideration of uncertainties caused by irregular cross-section is expected. On these bases, a combination of the modified Manning Equation and VHR method will generate more realistic initial values for the AMHG parameters, which will result in enhanced calculation efficiency and accuracy for the AMHG method.

Statement of authorship

ZC, XJ and YS designed the study; PT performed modelling work and analyzed output data; SY and GY collected data; HL and WZ performed the meta-analysis; ZC and PT wrote and revised the manuscript.

Acknowledgements

We acknowledge the reviewers and editors for their valuable advice on improving the quality of this paper. We thank the China Scholar Council (CSC) and our colleagues from Jinan Survey Bureau of Hydrology, and Beijing Normal University for their support in funding the research and collaboration during field investigations.

This research was jointly supported by the National Natural Science Foundation of China (grant numbers u1812401 & 41471340), the 111 Project (B18006), the National Key Project for R&D (grant numbers 2016YFC0402403 & 2016YFC0402409), and the Shaanxi Key Science and Technology Innovation Team Project (grant number 2014KCT-27), China.

References

Andreadis, K.M., Clark, E.A., Lettenmaier, D.P., Alsdorf, D.E., 2007. Prospects for river discharge and depth estimation through assimilation of swath-altimetry into a raster-based hydrodynamics model. Geophys. Res. Lett. 34 (10).

Barber, C.A., Gleason, C.J., 2018. Verifying the prevalence, properties, and congruent hydraulics of at-many-stations hydraulic geometry (AMHG) for rivers in the continental United States. J. Hydrol. 556, 625–633.

Bi, P., Zhang, Y., Parton, K.A., 2007. Weather variables and Japanese encephalitis in the metropolitan area of Jinan city, China. J. Infect. 55 (6), 551–556.

Biancamaria, S., Lettenmaier, D.P., Pavelsky, T.M., 2016. The SWOT Mission and its Capabilities for Land Hydrology Remote Sensing and Water Resources. Springer, pp. 117–147.

Birkinshaw, S., Moore, P., Kilsby, C., O'donnell, G., Hardy, A., Berry, P., 2014. Daily discharge estimation at ungauged river sites using remote sensing. Hydrol. Process. 28 (3), 1043–1054.

Bjerklie, D.M., Dingman, S.L., Bolster, C.H., 2005. Comparison of constitutive flow resistance equations based on the Manning and Chezy equations applied to natural rivers. Water Resour. Res. 41 (11).

Bjerklie, D.M., Birkett, C.M., Jones, J.W., Carabajal, C., Rover, J.A., Fulton, J.W., Garambois, P.A., 2018. Satellite remote sensing estimation of river discharge: application to the Yukon River Alaska. J. Hydrol. 561, 1000–1018.

Bonnema, M.G., Sikder, S., Hossain, F., Durand, M., Gleason, C.J., Bjerklie, D.M., 2016. Benchmarking wide swath altimetry-based river discharge estimation algorithms for the Ganges river system. Water Resour. Res. 52 (4), 2439–2461.

Chadalawada, J., Havlíček, V., Babovic, V., 2016. Genetic programming based approach towards understanding the dynamics of urban rainfall-runoff process. Procedia engineering 154, 1093–1102.

Chen, Q., Tao, H., Zhang, W., Li, Z., Zhang, P., 2017. Experiment and analysis of retrieving land surface parameters using polarization radar images in Genhe area of China. 2017 IEEE International Geoscience and Remote Sensing Symposium (IGARSS). IEEE, pp. 4968–4971 July.

Chlumecký, M., Buchtele, J., Richta, K., 2017. Application of random number generators in genetic algorithms to improve rainfall-runoff modelling. J. Hydrol. 553, 350–355.

Cho, S.-J., Bang, E.-S., Kang, I.-M., 2015. Construction of precise digital terrain model for nonmetal open-pit mine by using unmanned aerial photograph. Economic and Environmental Geology 48 (3), 205–212.

Choi, J., Yeom, J., Chang, A., Byun, Y., Kim, Y., 2012. Hybrid pansharpening algorithm for high spatial resolution satellite imagery to improve spatial quality. IEEE Geosci. Remote Sens. Lett. 10 (3), 490–494.

Chu, J., Fan, J., Chen, Y., Zhang, F., 2016. A comparative analysis on GF-2 remote sensing image fusion effects. 2016 IEEE International Geoscience and Remote Sensing Symposium (IGARSS). IEEE, pp. 3770–3773.

Colomina, I., Molina, P., 2014. Unmanned aerial systems for photogrammetry and remote sensing: a review. ISPRS J. Photogramm. Remote Sens. 92, 79–97.

Costa, J.E., Spicer, K.R., Cheng, R.T., Haeni, F.P., Melcher, N.B., Thurman, E.M., Plant, W.J., 2000. Measuring stream discharge by non-contact methods: a proof-of-concept experiment. Geophys. Res. Lett. 27 (4), 553–556.

Costa, J., Cheng, R., Haeni, F., Melcher, N., Spicer, K., Hayes, E., Teague, C., Barrick, D., 2006. Use of radars to monitor stream discharge by noncontact methods. Water Resour. Res. 42 (7).

De Jong, K.A., 1975. Analysis of the Behavior of a Class of Genetic Adaptive Systems.

Dhamge, N.R., Atmapoojya, S., Kadu, M.S., 2012. Genetic algorithm driven ANN model for runoff estimation. Procedia Technology 6, 501–508.

Dingman, S.L., 2009. Fluvial hydraulics. oxford university press.

Durand, M., Neal, J., Rodríguez, E., Andreadis, K.M., Smith, L.C., Yoon, Y., 2014. Estimating reach-averaged discharge for the River Severn from measurements of river water surface elevation and slope. J. Hydrol. 511, 92–104.

Durand, M., Gleason, C., Garambois, P.-A., Bjerklie, D., Smith, L., Roux, H., Monnier, J., 2016. An intercomparison of remote sensing river discharge estimation algorithms from measurements of river height, width, and slope. Water Resour. Res. 52 (6), 4527–4549.

Escartin, J., Aubrey, D., 1995. Flow structure and dispersion within algal mats. Estuar. Coast. Shelf Sci. 40 (4), 451–472.

Fei, Z., Li, B., Yang, S., Xing, C., Chen, H., Hanzo, L., 2017. A survey of multi-objective optimization in wireless sensor networks: metrics, algorithms, and open problems. IEEE Communications Surveys & Tutorials 19 (1), 550–586.

Feng, Y., Wang, G.G., Li, W., Li, N., 2017. Multi-strategy monarch butterfly optimization algorithm for discounted {0-1} knapsack problem. Neural Comput. & Applic. 1–18.

Ferguson, R., 2010. Time to abandon the Manning equation? Earth Surf. Process. Landf. 35 (15), 1873–1876.

Fonseca, C.M., Fleming, P.J., 1993. Genetic Algorithms for Multiobjective Optimization: Formulation Discussion and Generalization (Paper presented at the Icga).

Getirana, A.C.V., Peters-Lidard, C., 2013. Estimating water discharge from large radar altimetry datasets. Hydrol. Earth Syst. Sci. 17 (3), 923–933.

Gleason, C.J., Hamdan, A.N., 2015. Crossing the (watershed) divide: satellite data and the changing politics of international river basins. Geogr. J. 183 (1), 2–15.

Gleason, C.J., Smith, L.C., 2014. Toward global mapping of river discharge using satellite images and at-many-stations hydraulic geometry. Proc. Natl. Acad. Sci. 111 (13), 4788–4791.

Gleason, C.J., Wang, J., 2015. Theoretical basis for at-many-stations hydraulic geometry. Geophys. Res. Lett. 42 (17), 7107–7114.

Gleason, C.J., Smith, L.C., Lee, J., 2014. Retrieval of river discharge solely from satellite imagery and at-many-stations hydraulic geometry: sensitivity to river form and optimization parameters. Water Resour. Res. 50 (12), 9604–9619.

Gleason, C.J., Durand, M.T., Garambois, P.A., 2016. Forward to the future: Estimating river discharge with McFLI. AGU Fall Meeting Abstracts.

Gleason, C.J., Wada, Y., Wang, J., 2018. A hybrid of optical remote sensing and hydrological modeling improves water balance estimation. Journal of Advances in Modeling Earth Systems 10 (1), 2–17.

Goldberg, D.E., Holland, J.H., 1988. Genetic algorithms and machine learning. Mach. Learn. 3 (2), 95–99.
Gosling, S.N., Arnell, N.W., 2011. Simulating current global river runoff with a global hydrological model: model revisions, validation, and sensitivity analysis. Hydrol. Process. 25 (7), 1129–1145.
Hagemann, M.W., Gleason, C.J., Durand, M.T., 2017. BAM: Bayesian AMHG-manning inference of discharge using remotely sensed stream width, slope, and height. Water Resour. Res. 53 (11), 9692–9707.
Herman, M.R., Nejadhashemi, A.P., Abouali, M., Hernandez-Suarez, J.S., Daneshvar, F., Zhang, Z., Sharifi, A., 2018. Evaluating the role of evapotranspiration remote sensing data in improving hydrological modeling predictability. J. Hydrol. 556, 39–49.
Hirpa, F.A., Hopson, T.M., De Groeve, T., Brakenridge, G.R., Gebremichael, M., Restrepo, P.J., 2013. Upstream satellite remote sensing for river discharge forecasting: application to major rivers in South Asia. Remote Sens. Environ. 131, 140–151.
Holland, J.H., 1992. Genetic algorithms. Sci. Am. 267 (1), 66–73.
Horton, P., Jaboyedoff, M., Obled, C., 2017. Global optimization of an analog method by means of genetic algorithms. Mon. Weather Rev. 145 (4), 1275–1294.
Ielpi, A., 2017. Controls on sinuosity in the sparsely vegetated Fossálar River, southern Iceland. Geomorphology 286, 93–109.
Iqbal, A., Ullah, S., Khalid, N., Ahmad, W., Ahmad, I., Shafique, M., Hulley, G.C., Roberts, D.A., Skidmore, A.K., 2018. Selection of HyspIRI optimal band positions for the earth compositional mapping using HyTES data. Remote Sens. Environ. 206, 350–362.
Jung, H.C., Hamski, J., Durand, M., Alsdorf, D., Hossain, F., Lee, H., Azad Hossain, A.K.M., Hasan, K., Khan A., A., Hoque, A.Z., 2010. Characterization of complex fluvial systems using remote sensing of spatial and temporal water level variations in the Amazon, Congo, and Brahmaputra Rivers. Earth Surface Processes and Landforms: The Journal of the British Geomorphological Research Group 35 (3), 294–304.
Kankaku, Y., Suzuki, S., Osawa, Y., 2013, July. ALOS-2 mission and development status. 2013 IEEE International Geoscience and Remote Sensing Symposium-IGARSS. IEEE, pp. 2396–2399.
Karimkashi, S., Kishk, A.A., 2010. Invasive weed optimization and its features in electromagnetics. IEEE Transactions on Antennas & Propagation 58 (4), 1269–1278.
Konak, A., Coit, D.W., Smith, A.E., 2006. Multi-objective optimization using genetic algorithms: a tutorial. Reliability Engineering & System Safety 91 (9), 992–1007.
Lane, S.N., 2005. Roughness–time for a re-evaluation? Earth Surf. Process. Landf. 30 (2), 251–253.
Le Coz, J., Hauet, A., Pierrefeu, G., Dramais, G., Camenen, B., 2010. Performance of image-based velocimetry (LSPIV) applied to flash-flood discharge measurements in Mediterranean rivers. J. Hydrol. 394 (1–2), 42–52.
Lee, S., Choi, Y., 2015. Topographic survey at small-scale open-pit mines using a popular rotary-wing unmanned aerial vehicle (drone). Tunnel and Underground Space 25 (5), 462–469.
Lee, M.C., Leu, J.M., Lai, C.J., Plant, W.J., Keller, W.C., Hayes, K., 2002. Non-contact flood discharge measurements using an X-band pulse radar (II) improvements and applications. Flow Meas. Instrum. 13 (5–6), 271–276.
LeFavour, G., Alsdorf, D., 2005. Water slope and discharge in the Amazon River estimated using the shuttle radar topography mission digital elevation model. Geophys. Res. Lett. 32 (17).
Legleiter, C.J., Kinzel, P.J., Nelson, J.M., 2017. Remote measurement of river discharge using thermal particle image velocimetry (PIV) and various sources of bathymetric information. J. Hydrol. 554, 490–506.
Leopold, L.B., Maddock, T., 1953. The Hydraulic Geometry of Stream Channels and some Physiographic Implications. vol. 252. US Government Printing Office.
Leung, Y., Gao, Y., Xu, Z.B., 1997. Degree of population diversity-a perspective on premature convergence in genetic algorithms and its markov chain analysis. IEEE Trans. Neural Netw. 8 (5), 1165–1176.
Li, W., 2016. Near-field Remote Sensing of Riverine Hydrodynamic Processes With 3D Large Scale Particle Image Velocimetry.
Li, D.R., Chen, X.L., Cai, X.B., 2008. Spatial information techniques in rapid response to Wenchuan earthquake. Journal of Remote Sensing (6), 841–851.
Li, X., Liu, S.M., Ma, M.G., Xiao, Q., Liu, Q.H., Jin, R., Li, H.Y., 2012. HiWATER:an integrated remote sensing experiment on hydrological and ecological processes in the Heihe River basin. Adv. Earth Science 27 (5), 481–498.
Li, X., Epitropakis, M.G., Deb, K., Engelbrecht, A., 2016. Seeking multiple solutions: an updated survey on niching methods and their applications. IEEE Trans. Evol. Comput. 21 (4), 518–538.
Li, Z., Shahidehpour, M., Bahramirad, S., Khodaei, A., 2017. Optimizing traffic signal settings in smart cities. IEEE Transactions on Smart Grid 8 (5), 2382–2393.
López, R., Barragán, J., Colomer, M.À., 2007. Flow resistance equations without explicit estimation of the resistance coefficient for coarse-grained rivers. J. Hydrol. 338 (1–2), 113–121.
Lu, S.L., Wu, B.F., Yan, N.N., Li, F.P., Wen, M.P., W, J., 2010. Progress in river runoff monitoring by remote sensing. Advance in Earth Science 25 (8), 820–826.
Moriasi, D.N., Arnold, J.G., Van Liew, M.W., Bingner, R.L., Harmel, R.D., Veith, T.L., 2007. Model evaluation guidelines for systematic quantification of accuracy in watershed simulations. Trans. ASABE 50 (3), 885–900.
Nash, J.E., Sutcliffe, J.V., 1970. River flow forecasting through conceptual models part I—A discussion of principles. J. Hydrol. 10 (3), 282–290.
Neugirg, F., Stark, M., Kaiser, A., Vlacilova, M., Seta, M.D., Vergari, F., et al., 2016. Erosion processes in calanchi in the upper orcia valley, southern tuscany, Italy based on multitemporal high-resolution terrestrial lidar and uav surveys. Geomorphology 269, 8–22.
Nicolle, P., Pushpalatha, R., Perrin, C., François, D., Thiéry, D., Mathevet, T., et al., 2014. Benchmarking hydrological models for low-flow simulation and forecasting on french catchments. Hydrol. Earth Syst. Sci. 18 (8), 2829–2857 18,8(2014-08-05).
Nopiah, Z.M., Khairir, M.I., Abdullah, S., Baharin, M.N., Arifin, A., 2010. Time complexity analysis of the genetic algorithm clustering method. Wseas International Conference on Signal Processing, Robotics and Automation. World Scientific and Engineering Academy and Society (WSEAS), pp. 171–176.
Pan, F., Wang, C., Xi, X., 2016. Constructing river stage-discharge rating curves using remotely sensed river cross-sectional inundation areas and river bathymetry. J. Hydrol. 540, 670–687.
Pandey, H.M., Chaudhary, A., Mehrotra, D., 2014. A comparative review of approaches to prevent premature convergence in GA. Appl. Soft Comput. 24, 1047–1077.
Papa, F., Durand, F., Rossow, W.B., Rahman, A., Bala, S.K., 2010. Satellite altimeter-derived monthly discharge of the Ganga-Brahmaputra River and its seasonal to interannual variations from 1993 to 2008. Journal of Geophysical Research: Oceans 115 (C12).
Parent, E., Bernier, J., 2003. Bayesian POT modeling for historical data. J. Hydrol. 274 (1–4), 95–108.
Pavelsky, T.M., Durand, M.T., Andreadis, K.M., Beighley, R.E., Paiva, R.C., Allen, G.H., Miller, Z.F., 2014. Assessing the potential global extent of SWOT river discharge observations. J. Hydrol. 519, 1516–1525.
Pawłowski, D., Milecka, K., Kittel, P., Woszczyk, M., Spychalski, W., 2015. Palaeoecological record of natural changes and human impact in a small river valley in Central Poland. Quat. Int. 370, 12–28.
Pawłowski, D., Borówka, R.K., Kowalewski, G.A., Luoto, T.P., Milecka, K., Nevalainen, L., et al., 2016. Late weichselian and holocene record of the paleoenvironmental changes in a small river valley in Central Poland. Quat. Sci. Rev. 135, 24–40.
Pitz, W., Miller, D., 2010. The TerraSAR-X satellite. IEEE Trans. Geosci. Remote Sens. 48 (2), 615–622.
Reis Jr., D.S., Stedinger, J.R., 2005. Bayesian MCMC flood frequency analysis with historical information. J. Hydrol. 313 (1–2), 97–116.
Rudolph, G., 1994. Convergence analysis of canonical genetic algorithms. IEEE Trans. Neural Netw. 5 (1), 96–101.
Ruiz, J., Macías, D., Peters, F., 2004. Turbulence increases the average settling velocity of phytoplankton cells. Proc. Natl. Acad. Sci. 101 (51), 17720–17724.
Shen, C., Wang, S., Liu, X., 2016. Geomorphological significance of at many stations hydraulic geometry. Geophys. Res. Lett. 43 (8), 3762–3770.
Shen, X., Anagnostou, E.N., Allen, G.H., Brakenridge, G.R., Kettner, A.J., 2019. Near-real-time non-obstructed flood inundation mapping using synthetic aperture radar. Remote Sens. Environ. 221, 302–315.
Smith, L.C., Isacks, B.L., Forster, R.R., Bloom, A.L., Preuss, I., 1995. Estimation of discharge from braided glacial rivers using ERS 1 synthetic aperture radar: first results. Water Resour. Res. 31 (5), 1325–1329.
Smith, L.C., Isacks, B.L., Bloom, A.L., Murray, A.B., 1996. Estimation of discharge from three braided rivers using synthetic aperture radar satellite imagery: potential application to ungaged basins. Water Resour. Res. 32 (7), 2021–2034.
Song, P., Liu, Y.B., Liu, Y.C., 2011. Advances in satellite retrieval of terrestrial surface water parameters. Adv. Earth Science 26 (7), 731–740.
Sozzi, M., Marinello, F., Pezzuolo, A., Sartori, L., 2018. Benchmark of satellites image services for precision agricultural use. Proceedings of the AgEng Conference, Wageningen, the Netherlands, pp. 8–11.
Srinivas, M., Patnaik, L.M., 1994. Adaptive probabilities of crossover and mutation in genetic algorithms. IEEE Transactions on Systems, Man, and Cybernetics 24 (4), 656–667.
Sun, D.P., 2007. "Eleventh Five-Year" National Planning Textbook for General Higher Education, Hydraulic.
Toth, C., Jóźków, G., 2016. Remote sensing platforms and sensors: a survey. ISPRS J. Photogramm. Remote Sens. 115, 22–36.
Tsoukalas, I., Kossieris, P., Efstratiadis, A., Makropoulos, C., 2016. Surrogate-enhanced evolutionary annealing simplex algorithm for effective and efficient optimization of water resources problems on a budget. Environ. Model Softw. 77, 122–142.
Vatankhah, A.R., Ghafari, S., Mazdeh, A.M., 2015. New and improved hydraulic radius for channels of the second kind. Ain Shams Engineering Journal 6 (3), 767–773.
Vivoni, E.R., Rango, A., Anderson, C.A., Pierini, N.A., Schreiner-McGraw, A.P., Saripalli, S., Laliberte, A.S., 2014. Ecohydrology with unmanned aerial vehicles. Ecosphere 5 (10), 1–14.
Voinov, A.A., Voinov, H., Costanza, R., 1999. Surface water flow in landscape models: 2. Patuxent watershed case study. Ecol. Model. 119 (2–3), 211–230.
Vörösmarty, C.J., Willmott, C.J., Choudhury, B.J., Schloss, A.L., Stearns, T.K., Robeson, S.M., Dorman, T.J., 1996. Analyzing the discharge regime of a large tropical river through remote sensing, ground-based climatic data, and modeling. Water Resour. Res. 32 (10), 3137–3150.
Watts, A.C., Ambrosia, V.G., Hinkley, E.A., 2012. Unmanned aircraft systems in remote sensing and scientific research: classification and considerations of use. Remote Sens. 4 (6), 1671–1692.
Wei, Haicheng, Xiao, Mingxia, Zhu, Ling, Miaojun, W., Xing, W., Zhang, Xiuxia, Zhang, Bai, 2016. Study on monitoring technology of UAV aerial image enhancement for burning straw. 2016 Chinese Control and Decision Conference (CCDC). IEEE, pp. 4321–4325 May.
Westerberg, L.-O., Hagberg, E., 2018. Geomorphology and pedology of the Engaruka archaeological environment, Tanzania, and the effects of the 1997–1998 El Niño flash-flood. CATENA 163, 244–256.
Woo, J., Son, K., Li, T., Kim, G.S., Kweon, I.S., 2007. Vision-Based UAV Navigation in Mountain Area. MVA, pp. 236–239 May.
Wu, H., Li, Z.L., 2009. Scale issues in remote sensing: a review on analysis, processing and modeling. Sensors 9 (3), 1768–1793.
Xu, K., Zhang, J., Watanabe, M., Sun, C., 2004. Estimating river discharge from very high-resolution satellite data: a case study in the Yangtze River, China. Hydrol. Process. 18 (10), 1927–1939.

Zhang, J.Q., Xu, K.Q., Watanabc, M., 2002. Estimation of river discharge using very high-resolution satellite data in Yangtze River. Proceedings of International Symposium on Remote Sensing. Sokcho, Korea, pp. 728–733.
Zhang, J.Q., Xu, K.Q., Gui, S.Z., Chen, X.W., Sun, C.P., 2004. Estimation of river discharge using TOPEX/Poseidon altimeter data. Acta Geograph. Sin. 59 (1), 95–100.
Zhang, X., Srinivasan, R., Bosch, D., 2009. Calibration and uncertainty analysis of the swat model using genetic algorithms and Bayesian model averaging. J. Hydrol. 374 (3), 307–317.
Zhang, C.B., Yang, S.T., Zhao, C.S., Lou, H.Z., Zhang, Y.C., Bai, J., Zhang, Y., 2018. Topographic data accuracy verification of small consumer UAV. Journal of Remote Sensing 22 (01), 185–195 2018.
Zhou, J., Broodbank, N., 2014. Sediment-water interactions of pharmaceutical residues in the river environment. Water Res. 48, 61–70.